Characterizing earthquake recurrence parameters for offshore faults in the low strain, compressional Kapiti-Manawatu Fault System, New Zealand

Scott Nodder, Geoffroy Lamarche, Jean-Noël Proust, Mark Stirling

Characterizing earthquake recurrence parameters for offshore faults in the low-strain, compressional Kapiti-Manawatu Fault System, New Zealand

Scott D. Nodder,[1] Geoffroy Lamarche,[1] Jean-Noël Proust,[2] and Mark Stirling[3]

Received 20 February 2007; revised 16 August 2007; accepted 4 September 2007; published 29 December 2007.

[1] Seafloor fault scarps and near-surface deformation of late Quaternary seismic reflectors occur along the eastern margin of the Wanganui Basin, 200 km behind the active Hikurangi subduction front, southern North Island, New Zealand. The offshore scarps are associated with the low-strain, compressional Kapiti-Manawatu Fault System (KMFS), which comprises high-angle (>60°) reactivated reverse and normal faults oriented NE-SW, highly oblique to the coast. Seafloor scarps range from <10 to 50 km in length with vertical seafloor offsets of 2 to 30 m. The longest structure is the Mascarin Fault, with maximum late Quaternary vertical slip rates of 3 mm a^{-1} (where a is years). Other faults in the KMFS have typical rates of <1 mm a^{-1}, comparable to long-term estimates. Three zones of recent deformation are identified: faults in the north and south of the KMFS are characterized by high scarps (>10 m high) and moderate to long fault seafloor rupture lengths, and those in central parts of the fault system are characterized by low scarps (<5 m high), variable slip rates, and short to moderate fault lengths. Empirical equations indicate that KMFS faults may generate earthquakes with moment magnitudes (M_w) of 5.7–7.5 (mean 6.9 ± 0.3, ±1 standard deviation, for sources with $M_w \geq 6.5$). Estimated recurrence intervals that are generally >10,000 a, suggest that the seismic hazard of the Kapiti-Manawatu region is relatively low. Incorporation of these new geological data, however, is likely to increase slightly the expected seismic hazard in southern North Island. The method of determining the earthquake recurrence parameters of offshore faults has potentially wider applications elsewhere.

Citation: Nodder, S. D., G. Lamarche, J.-N. Proust, and M. Stirling (2007), Characterizing earthquake recurrence parameters for offshore faults in the low-strain, compressional Kapiti-Manawatu Fault System, New Zealand, *J. Geophys. Res.*, *112*, B12102, doi:10.1029/2007JB005019.

1. Introduction

[2] The first stages of seismic hazard and risk assessments are (1) the identification and characterization of active earthquake sources and (2) the quantification of earthquake recurrence rates on these sources [*Cornell*, 1968; *Schwartz and Coppersmith*, 1986; *DePolo and Slemmons*, 1990]. The seismic hazard associated with active faults and folds can be quantified by combining these data with historical seismicity and local ground-shaking characteristics using probabilistic modeling techniques [e.g., *Wesnousky*, 1986; *Stirling et al.*, 1998, 2002b]. Such approaches are applied most readily to onshore environments where the neotectonic characteristics of faults and rupture characteristics of specific earthquake sources can be evaluated using paleoseismic [e.g., *Schwartz and Coppersmith*, 1986; *DePolo and Slemmons*, 1990; *van Dissen and Berryman*, 1996] and empirical techniques [*Bonilla et al.*, 1984; *Wells and Coppersmith*, 1994; *Anderson et al.*, 1996; *Stirling et al.*, 2002a]. In coastal zones, however, the potential seismic hazard and risk can be underestimated without consideration of the distribution and rupture characteristics of active faults and folds that are either entirely or partially offshore [e.g., *Wesnousky*, 1986; *Nodder*, 1994].

[3] At subduction margins, deformation occurs predominantly in the fore-arc basin but can also extend a considerable distance away from the subduction front into the back-arc environment [e.g., *Busby and Ingersoll*, 1995]. An example is described here from the predominantly reverse, offshore Kapiti-Manawatu Fault System (KFMS), North Island, New Zealand, which is located approximately 200 km west of and behind the active deformation front of the Hikurangi subduction margin, along the eastern edge of the Wanganui Basin (WB) (Figure 1). The KMFS is associated laterally with onland structures that have previously been identified as potential earthquake sources (e.g., Manawatu Anticlines [*Te Punga*, 1957; *Melhuish et al.*, 1996]) and previous paleoseismic studies in southern North

[1] National Institute of Water and Atmospheric Research Ltd, Wellington, New Zealand.
[2] Géosciences Rennes, UMR CNRS 6118, Université de Rennes 1, Rennes, France.
[3] Institute of Geological and Nuclear Sciences Ltd, Lower Hutt, New Zealand.

0148-0227/07/2007JB005019$09.00

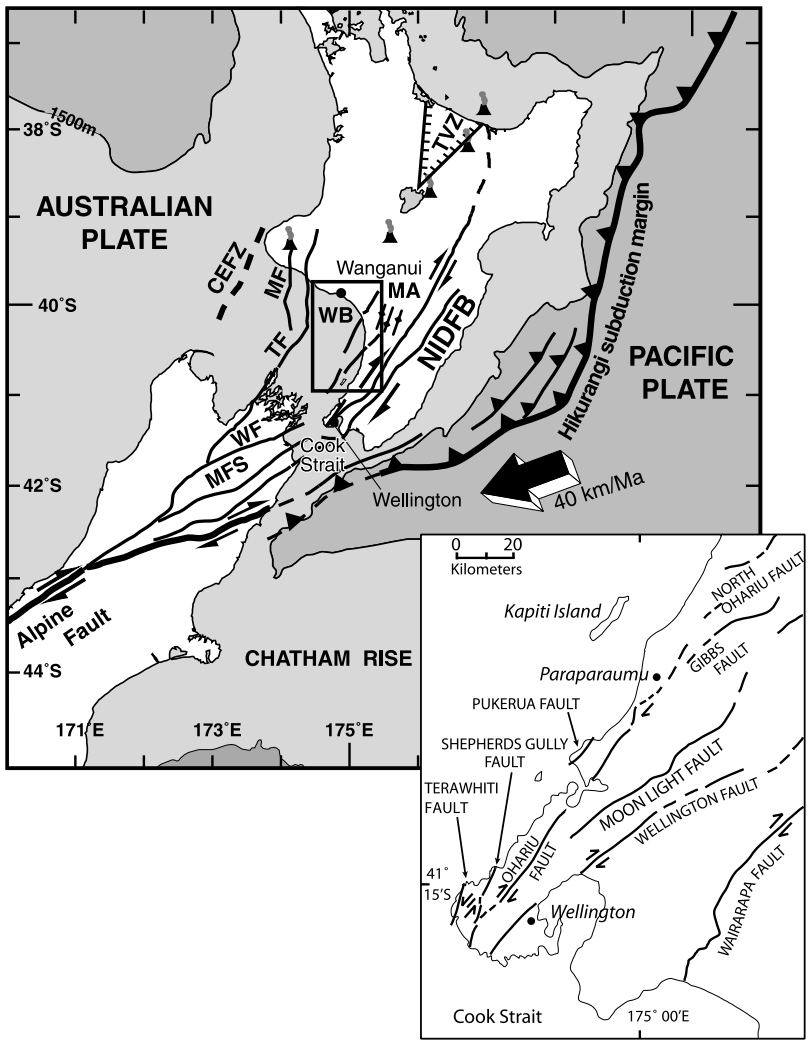

Figure 1. Regional location and fault map of the Wanganui Basin (WB) and offshore Kapiti-Manawatu Fault System along the eastern edge of the basin. The Hikurangi subduction front is shown by the toothed line, marking the boundary between the Pacific and Australian plates. The large arrow shows the relative plate motion (in km Ma^{-1}) from *De Mets et al.* [1994]. Bold lines indicate other major geological faults and folds, including the Manawatu Anticlines (MA). TVZ, Taupo Volcanic Zone; NIDFB, North Island Dextral Fault Belt; CEFZ, Cape Egmont Fault Zone; MF, Manaia Fault; TF, Taranaki Fault; MFS, Marlborough Fault System; WF, Wairau Fault and the Alpine Fault. Active volcanoes are also shown. Box outline shows the position of Figure 2. The inset shows in detail the active strike-slip faults in the onshore Wellington region [after *van Dissen and Berryman*, 1996; *Litchfield et al.*, 2004].

Island have identified a number of onshore active faults [*Smith and Berryman*, 1986; *van Dissen and Berryman*, 1996; *Stirling et al.*, 1998, 2002b]. These predominantly land-based studies, however, have failed to take into account the late Quaternary activity of offshore faults because structures in the marine environment have only been mapped previously at basin-wide scales using low-resolution geophysical techniques [*Anderton*, 1981; *Carter et al.*, 1988; *Lewis et al.*, 1994]. This is likely to result in a slight underestimation of the seismic hazard in southern North Island, as was observed previously by *Wesnousky* [1986] in a study offshore California. The present study utilizes a suite of high-resolution, subsurface seismic reflection and core data, and recent interpretations of fault structure and stratigraphy in the KMFS [*Lamarche et al.*, 2005; *Proust et al.*, 2005] to constrain the late Quaternary to post-20 ka (where a is years) activity on these offshore faults with a view to better evaluating the seismic hazard and risk implications for southern North Island.

[4] The principal objectives of this study are (1) to describe in detail the neotectonic pattern of the low-strain, compressional, offshore KMFS, (2) to identify and characterize seismogenic faults, i.e., those that are capable of generating earthquakes, (3) to estimate earthquake source parameters, such as fault length, area, and slip rate, and (4) to evaluate earthquake recurrence parameters, such as moment magnitude, seismic moment, single-event displacement, and recurrence interval, associated with these faults using published empirical relationships developed initially for appraising onshore earthquake hazards. The relevance of

this approach for evaluating the earthquake recurrence characteristics of offshore faults has wider applicability than is currently reflected in the literature, in which most published studies are from New Zealand [e.g., *Nodder*, 1994; *Barnes et al.*, 2002; *Bull et al.*, 2006]. In the context of the present study, "neotectonics" encompasses deformation since the initiation of contractional tectonics in the KMFS, which is estimated to be about 1.35–2.4 Ma [*Lamarche et al.*, 2005; *Proust et al.*, 2005], and considers "active" structures within the fault system to be those that have deformed sedimentary layers that are no more than 20,000 a old and/or are characterized by the presence of a seafloor scarp.

2. Geological Setting

[5] The WB is a 4–5 km deep, Plio-Pleistocene sedimentary basin lying between 39°50′S and 41°S wholly on the Australian Plate about 200 km west of the southern part of the Hikurangi subduction front, where the Pacific Plate is being subducted obliquely beneath the North Island of New Zealand [*Anderton*, 1981; *Katz and Leask*, 1990; *Stern et al.*, 1992, 1993; *Proust et al.*, 2005] (Figure 1). Modeling and basin-scale deformation patterns suggest that the basin has evolved over the last 3 Ma in response to substantial sediment loading and strong frictional coupling between the subducting Pacific Plate and the overriding Australian Plate [*Stern et al.*, 1992, 1993].

[6] The WB is bounded by uplifted Mesozoic basement highs with the buried Patea-Tongaporutu High and associated reverse Taranaki Fault [*Mills*, 1990; *Proust et al.*, 2005] lying along the western margin of the basin and the recently uplifted and overthrust (<1–2 Ma [*Lamb and Vella*, 1987]) North Island Axial Ranges to the east. The Plio-Pleistocene sedimentary basin fill comprises at least 4 km of predominantly shallow marine, cyclothemic sediments [*Fleming*, 1953; *Anderton*, 1981; *Carter and Naish*, 1998; *Naish et al.*, 1999; *Kamp et al.*, 2002; *Proust et al.*, 2005].

2.1. Active Faulting in Southern North Island

[7] Upper crustal faulting in the lower North Island is dominated by the North Island Dextral Fault Belt (NIDFB), which is located along the inner margin of the Hikurangi subduction margin and forearc basin [*Walcott*, 1987; *Beanland*, 1995] (Figure 1). The southern section of the NIDFB comprises a series of reverse and strike-slip faults that have facilitated the uplift of the North Island Axial Ranges and have been the sources for several large historic earthquakes (e.g., 1855 Wairarapa, M_w 8.2; 1931 Napier, M_w 7.8; 1934 Pahiatua, M_w 7.4 [*Grapes and Downes*, 1997; *Doser and Webb*, 2003]). West of the NIDFB, several active dextral strike-slip faults have been identified running subparallel to the west coast of southern North Island along the eastern margin of the WB [*van Dissen and Berryman*, 1996]. The Shepherds Gully, Pukerua, Ohariu and North Ohariu faults (Figure 1, insert) have estimated strike-slip rates of 1–3 mm a^{-1}, single-event displacements of 3–5 m and earthquake recurrence intervals of 1500–7000 a [*van Dissen and Berryman*, 1996; *Heron et al.*, 1998; *Litchfield et al.*, 2004]. An average moment magnitude (M_w) of 7.6 ± 0.3 was calculated for these faults [*van Dissen and Berryman*, 1996]. Furthermore, a series of normal and reverse faults [*Aharoni*, 1991] underlie the extensive 4–5 km wide Holocene coastal plain on the eastern edge of the WB between the Manawatu coast and the foot of the Axial Ranges to the east [*Cowie*, 1963; *Muckersie and Sheperd*, 1995].

[8] Several large reverse faults and active anticlinal structures have also been mapped, namely the Turakina, Rangitikei, and Rauoterangi faults [*Anderton*, 1981], the Manawatu Anticlines [*Fleming*, 1953; *Te Punga*, 1957; *Melhuish et al.*, 1996] and the offshore KMFS (see below [*Lamarche et al.*, 2005] (Figures 1 and 2). It has been postulated that these predominantly reverse faults have a component of dextral strike slip due to the interpreted en echelon pattern of faulting [*Anderton*, 1981; *Thompson et al.*, 1994], but this has not been corroborated by stress tensor modeling [*Stern et al.*, 1992] nor substantiated by fault geometry, as interpreted from marine seismic reflection studies [*Lamarche et al.*, 2005]. It is probable, however, that the KMFS reverse faults accommodate an as-yet undetermined amount of oblique-slip. Active growth on the anticlines in Manawatu is attributed to subsurface reverse faulting [*Te Punga*, 1957]. Average dip-slip rates on the west dipping, reverse fault responsible for uplift of the Mount Stewart-Halcombe Anticline are estimated at 0.1–0.2 mm a^{-1}, with a long-term late Quaternary (<0.2 Ma) deformation rate of 0.3 mm a^{-1} [*Melhuish et al.*, 1996]. On the basis of fold axis lengths of 15–20 km, *Jackson et al.* [1998] speculated that these faults would be capable of generating earthquakes of M_w 6.5–7.0.

[9] Offshore, the northern extension of the Wairau Fault from the northern part of South Island has been postulated to lie across western Cook Strait and to the west of Kapiti Island (Figure 1) [*Carter et al.*, 1988; *Moore and Francis*, 1988], perhaps linking with the Rauoterangi Fault in onshore Manawatu (Figure 2) [*Lewis et al.*, 1994]. The Wairau Fault represents the oldest extension of the major intracontinental strike-slip Alpine Fault, which is the largest single geological structure in New Zealand (Figure 1). In northern South Island, the Wairau Fault has an average late Quaternary slip rate of approximately 4 ± 1 mm a^{-1} and an average recurrence interval of 1000–2300 a, based on single-event horizontal displacements of 5–7 m [*van Dissen and Berryman*, 1996]. There are presently no data that allow us to determine the recent deformation history of the offshore section of the Wairau Fault because its location has still yet to be delineated [*Lamarche et al.*, 2005]. Consequently, this remains an outstanding issue for seismic hazard interpretations for the lower North Island region [e.g., *van Dissen and Berryman*, 1996; *Stirling et al.*, 1998, 2002b].

2.2. Fault Patterns and Long-Term Slip Rates in the Kapiti-Manawatu Fault System

[10] The first documentation of recent offshore faulting in the WB region was probably by *Fleming* [1953], who showed an abrupt drop in the seafloor aligned with the Nukumaru Fault in the central part of the basin from a single echo sounder trace. Other workers, such as *Anderton* [1981], *Thompson et al.* [1994], T. A. Stern and various coauthors [e.g., *Stern and Davey*, 1989; *Holt and Stern*, 1994; *Stern et al.*, 1992, 1993; *Proust et al.*, 2005] mapped basement structures and Plio-Pleistocene reflectors in off-

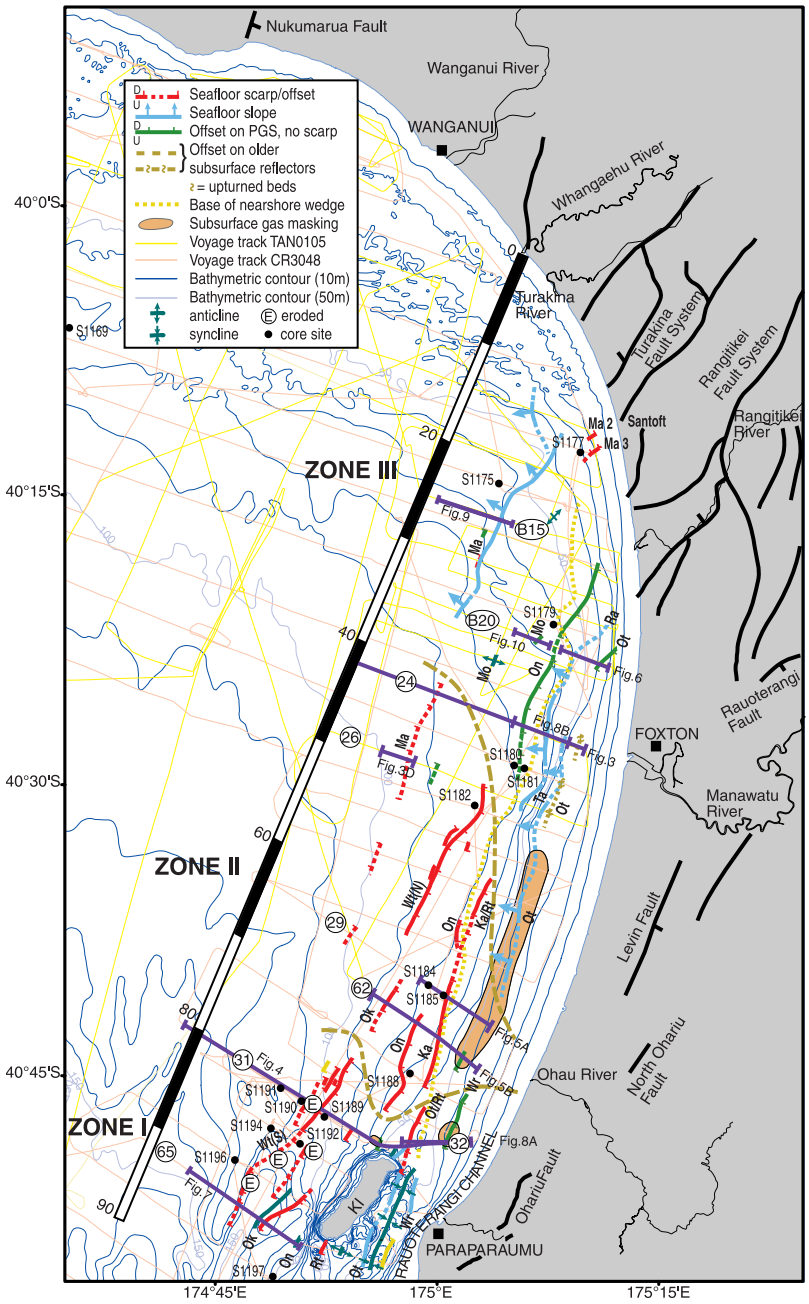

Figure 2. Neotectonic deformation map of the Kapiti-Manawatu Fault System (KMFS) showing the distribution of seafloor scarps and other surface and subsurface deformation. In the legend, PGS refers to the post-last glacial erosion surface (see text for details) and the circled E indicates where scarps are eroded. KI, Kapiti Island. Fault designations: Wt, Waitarere (S, southern section; N, northern); Ok, Okupe; On, Onepoto; Rt, Rangatira; Ot, Otaheke; Wr, Wairaka; Ka, Kapiti; Ma, Mascarin (Ma2, splay 2; Ma3, splay 3); Mo, Moana; Ra, Rangitikei; Ta, Tangimoana. Survey tracks from NIWA voyages CR3048 and TAN0105 are shown in orange and yellow, respectively, with track labels in circles. Locations of seismic reflection profiles in Figures 3–9 and core sites (solid dots) are indicated. The Santoft well location was used for previous stratigraphic correlations on multichannel seismic reflection profiles [*Lamarche et al.*, 2005; *Proust et al.*, 2005]. Bathymetric contours are shown in meters (light grey, every 10 m; blue, every 50 m). The N23°E projection axis for all the faults in the KMFS is also shown with marks every 10 km. The structural zones recognized by this paper are also depicted (zones I, II, and III).

shore WB using industrial seismic reflection data, but did not investigate near-surface, neotectonic deformation in the basin.

[11] *Lamarche et al.* [2005] described and mapped the 20–25 km wide offshore Kapiti-Manawatu Fault System (KMFS) in detail for the first time, and these results form the basis for the present study. The fault system extends from Kapiti Island in the south for 70–80 km to the mouths of the Turakina and Whangaehu rivers in the north (Figures 1 and 2). Twenty individual faults have been identified in the KMFS, comprising mainly steeply dipping (>60°), reactivated reverse faults with normal faults restricted predominantly to the southeastern and coastal edge of the fault system (Figures 2–4). The faults have an average strike direction of N20–30°E, subparallel to the Kapiti-Manawatu coast. The western boundary of the KMFS is usually marked by the major east dipping, reverse Mascarin Fault, which is the longest fault in the system (up to ~95 km in length). The Mascarin Fault probably extends further to the south of the study area and onland to the north where it possibly connects in a series of fault splays associated with the Turakina Fault System (Figure 2).

[12] From west to east across the KFMS, other significant reverse structures include the Waitarere, Okupe, Onepoto, Otaheke and Rangitikei faults (Figures 2–4). In close proximity to the two latter faults, the Kapiti Fault is a very steep normal fault characterized by large basement offsets of 400–600 m. The dominant easternmost fault in the KFMS, the Otaheke Fault, is a composite structure, which exhibits normal behavior south and east of Kapiti Island, but is a reverse structure to the northeast of the island. Normal faults are located further inshore from here, namely, Rangatira, Wairaka and Te Horo faults near Kapiti Island in the south and the Tangimoana Fault in the north (Figure 2).

[13] Time-vertical displacement plots for each of the main faults within the KMFS indicate that contractional deformation was initiated at 1.75 ± 0.40 Ma with fault growth rates in the order of ~1–2 mm a^{-1} and little to no accumulation of displacement occurring between 2.4 and 1.35 Ma [*Lamarche et al.*, 2005] (Figures 3c and 4b). Between 1.35 Ma and 120 ka, typical long-term slip rates were ~0.5 mm a^{-1}, increasing to rates >1 mm a^{-1} since 120 ka on the larger faults (e.g., Mascarin, Rangitikei). There is a possibility, however, that the age of the shallowest reflector in multichannel seismic reflection data might be considerably older than 120 ka (i.e., ~260 ka [*Proust et al.*, 2005]), which would result in more consistent deformation rates of 1.5 mm a^{-1} since 1.35 Ma [*Lamarche et al.*, 2005]. Lower slip rates are inferred on other KMFS faults over the same time periods, typically reaching maximum rates of 0.25–0.5 mm a^{-1}. Close spatial relationships between fault terminations on individual faults over different time horizons suggest that while not independently diagnostic of such phenomena, there has been limited lateral propagation of these faults since 1.35 Ma and in many cases for at least the last 2.4 Ma.

2.3. Historical Seismicity in the Wanganui Basin

[14] The WB is a zone of crustal seismicity, related primarily to the subduction of the Pacific Plate beneath the basin, with earthquakes occurring throughout the crust down to 40 km [*Robinson*, 1986]. Hypocentral locations and seismic reflection data define the Benioff Zone at the top of the subducted slab at depths of 30–40 km [*Robinson*, 1986; *Stern and Davey*, 1989; *Stern et al.*, 1992; *Ansell and Bannister*, 1996; *Reyners*, 1998]. Seismological and geodetic evidence indicates that the subduction interface is presently ''locked'' beneath the NIDFB and the Axial Ranges, immediately to the east of the WB, on timescales of at least 100 a [*Robinson*, 1986; *Walcott*, 1987; *Nicol and Beavan*, 2003].

[15] The high level of crustal seismicity in the WB is attributed to low heat flux in the crust [*Stern et al.*, 1992]. The Wanganui-Manawatu-Kapiti region is recognized for continuous, swarm-like shallow seismicity, typified by magnitudes of <5 and concentrating mostly offshore close to Wanganui city [*Garrick and Gibowicz*, 1983], with diffuse seismicity along the Kapiti-Manawatu coast. The area has been the scene of at least one large, historic earthquake near to Wanganui in 1897 (M 7 [*Eiby*, 1968] and M 6.5 (G. Downes and D. J. Dowrick, manuscript in preparation, 2007, also personal communication, 2006)). *Eiby* [1968] also indicated that an inferred M 7.5 earthquake in 1843 occurred near Wanganui, but this event has probably been mislocated and is likely to have an east coast, North Island source (G. Downes, personal communication, 2005). Composite fault plane solutions for small shallow earthquake (magnitude <3.5, crustal depth <12 km) from 1964 to 1980 indicate normal focal mechanisms with the axes of horizontal tension aligned approximately east–west [*Garrick and Gibowicz*, 1983]. In contrast, focal mechanisms for larger, and deeper (crustal depth ≤33 km) earthquakes indicate reverse faulting with a component of strike slip. Although the reasons for these contrasting earthquake events are not elucidated fully, compressional and extensional stresses may be generated above a bending lithospheric plate, causing normal faulting (bending moment faults) at the surface with reverse faulting occurring at depth [e.g., *Yeats*, 1986]. This is consistent with the presence of active extensional and contractional structures in the upper crust along the KMFZ as identified by *Lamarche et al.* [2005].

3. Methods

3.1. Seismic Reflection Data

[16] The present study is based on interpretation of a network of high-resolution, shallow subsurface seismic

Figure 3. Structural style and faults in the Kapiti-Manawatu Fault System (KMFS). (a) Uninterpreted northern transect, MCS TAN0105-24. (b) Interpreted profile with seafloor (sf), prominent unconformities (h1-5) and acoustic basement (B) shown. (c) Horizon age and vertical displacement of KMFS faults shown on the MCS profile in Figure 3a [after *Lamarche et al.*, 2005]. (d) Detail of MCS TAN0105-26 showing monoclinic fault drag of reflectors over the Mascarin Fault and inclined reflectors formed in the accommodation space created by faulting in the footwall. Profile locations are shown on Figure 2.

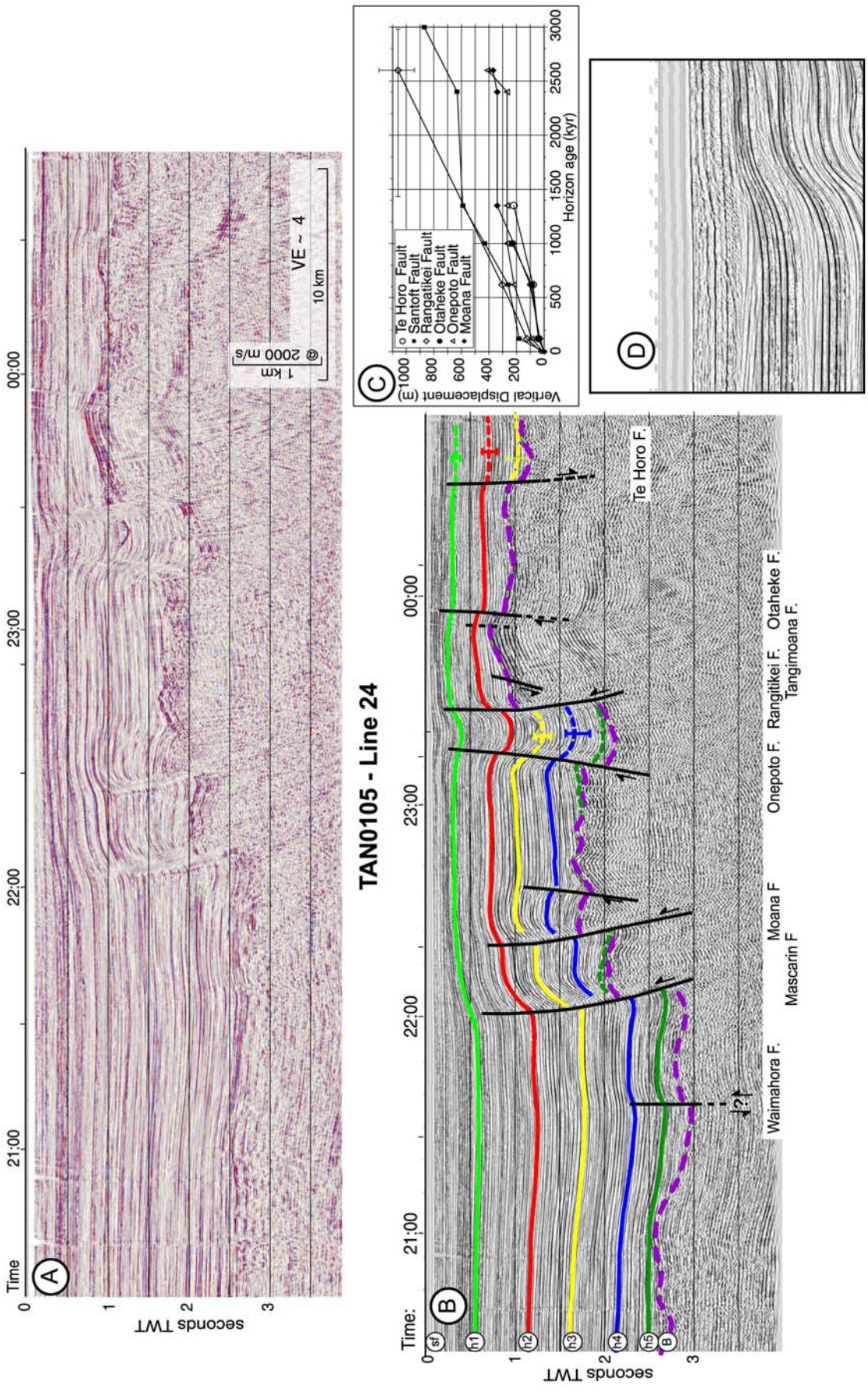
A
Time
21:00
22:00
23:00
00:00
seconds TWT
1 km
@ 2000 m/s
10 km
VE ~ 4
B
TAN0105 - Line 24
Time:
Te Horo F.
Onepoto F.
Rangitikei F.
Otaheke F.
Tangimoana F.
Moana F
Mascarin F
Waimahora F.
sf
h1
h2
h3
h4
h5
B
C
Vertical Displacement (m)
Horizon age (kyr)
Te Horo Fault
Santoft Fault
Rangatikei Fault
Otaheke Fault
Onepoto Fault
Moana Fault
D

Figure 3

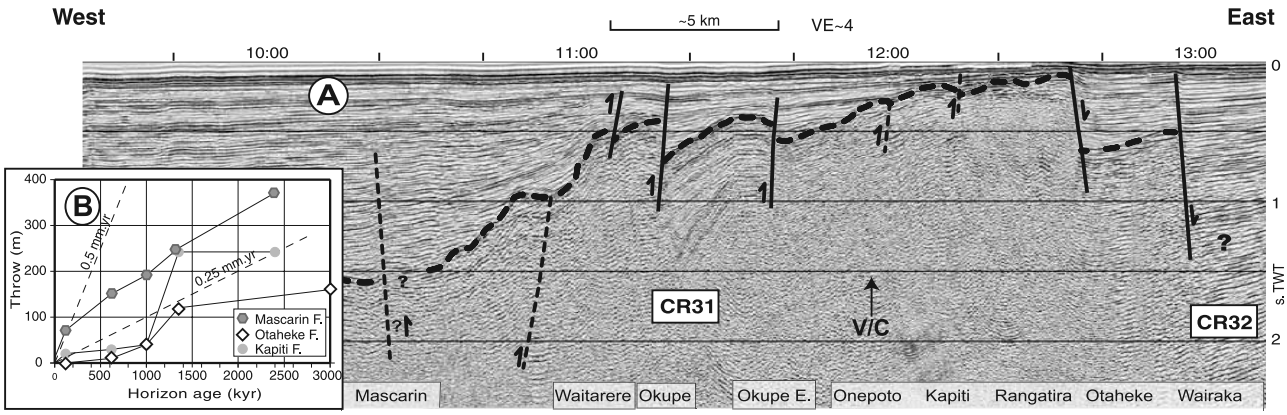

Figure 4. (a) Southern transect; MCS profile CR3048-line 31. The thick dashed line indicates the top of acoustic basement while the thinner, near-vertical dashed lines are inferred basement faults. V/C, variation in course of survey vessel during geophysical data acquisition. (b) Horizon age and vertical displacement of KMFS faults on the profile in Figure 4a [after *Lamarche et al.*, 2005]. Throw rates at 0.5 and 0.25 mm a^{-1} are shown for comparison. Profile locations are shown on Figure 2.

reflection profiles over the offshore KMFS acquired by NIWA in 1998 (survey CR3048, November) and 2001 (survey TAN0105, April) (Figure 2). The data utilized in this study are 3.5 kHz and Uniboom profiles, which were complemented by deeper, lower resolution, multichannel seismic reflection (MCS) data collected along the same tracks [*Lamarche et al.*, 2005; *Proust et al.*, 2005]. MCS data were of too low resolution to provide useful constraints on near-surface deformation but do provide valuable information on fault geometry, long-term deformation rates and possible fault interactions at depth. Across the study area, a maximum line spacing of 3 km and an average of 1.5 km was achieved within the seismic grid. Details regarding the data acquisition, processing and interpretation of the MCS profiles are given by *Lamarche et al.* [2005] and *Proust et al.* [2005].

[17] The high-resolution, shallow penetration seismic reflection data were acquired using a hull-mounted, 16-transducer ORE 3.5 kHz seismic profiler on all lines and a towed Uniboom source on a selected number of lines primarily along the Manawatu coast (Figure 2). The Uniboom had a nominal frequency of 1.2 kHz and a maximum penetration of 120 milliseconds (ms) two-way traveltime, while the 3.5 kHz had a penetration of no more than 75 ms. Uniboom data were filtered for the swell effects to improve subsurface resolution of the profiles, and no tidal corrections were made since tidal ranges in the Wanganui-Manawatu area are generally <1 to 1.5 m. The 3.5 kHz data were not postprocessed. No data were acquired in water depths shallower than 15 m.

3.2. Core Samples and Dating

[18] On the basis of shipboard interpretation of 3.5 kHz profiles, a piston corer was used to collect sediment core material for biostratigraphic (nannofossil) and radiocarbon dating in order to constrain recent fault movements using deformation of the post-last glacial erosion surface (PGS) (Figure 2). The PGS is a diachronous erosional surface that formed during the marine transgression following sea level lowering at the peak of the last glacial low stand 18–20 ka ago [*Carter et al.*, 1986 *Proctor and Carter*, 1989; *Pillans et al.*, 1993]. This surface is recognized widely across the New Zealand continental shelf [*Herzer*, 1981; *Nodder*, 1994] and provides an excellent time marker, provided that the amount of subsidence or uplift since its formation can be accounted for to allow the diachronous age of PGS to be estimated at different locations on the shelf [*Lamarche et al.*, 2006]. Ages of other younger reflective surfaces in the study area were also determined using similar techniques with radiocarbon dating providing absolute ages, compared with less well resolved nannobiostratigraphic data, which only provided broad age ranges and paleoenvironmental information (Tables 1 and 2).

3.3. Fault Geometry

[19] High-resolution seismic reflection data were used to locate seafloor fault scarps and characterize recent deformation of subsurface sedimentary units, aided by the distribution of faults on the 1.35 Ma stratigraphic horizon determined using MCS data [*Lamarche et al.*, 2005]. Scarp heights were measured on geophysical profiles assuming a speed of sound in seawater of 1500 m s^{-1} while vertical offsets on subsurface reflectors were estimated based on a speed of sound in late Quaternary sediments of 1600 m s^{-1} [e.g., *Nodder*, 1994]. Seafloor and subsurface offsets were measured directly from 3.5 kHz and boomer profiles, and, unless stated, are given in meters. The fault displacement data presented here assume that the faults are steep (>70°), as estimated from depth-converted MCS profiles, and may steepen toward the sediment surface [*Lamarche et al.*, 2005]. Interpretation of faults on MCS profiles can only provide information on dip-slip displacement on the fault plane, so that oblique- or strike-slip displacements cannot be estimated in this study.

[20] Fault rupture lengths in the KMFS were estimated from the lateral extent of fault surface expression, as represented primarily by mapped seafloor scarps and secondly by offsets of the PGS (Figure 2). Fault area was estimated from fault length and width, where fault width was derived from the inferred seismogenic depth of the fault

Table 1. Radiocarbon Age Determinations on Selected Core Samples From the Kapiti-Manawatu Fault System

NIWA Station	Water Depth, m	Latitude South	Longitude East	Sample Depth, cm	Sample Type[a]	Shell Identifications[b]	Laboratory Number[c]	^{14}C Age,[d] ^{14}C a B.P.	^{14}C Age,[e] calendar years B.P.	^{14}C Age Range (2σ)[d]	δ^{13}C, ‰ With Respect to PDB	Sediment Type and Core Depth
S1169	71	40°06.208′	174°32.431′	69	Shell - ^{14}C	*Talochlamys gemmulata* (JG/AMcI)	Wk7385	8810 ± 60	9211	9118–9406	2.3 ± 0.2	dark grey shelly silty sand, fining upward to shelly sandy silt; core depth 79 cm
S1175	56	40°14.384′	175°04.111′	39	Shell - ^{14}C	probably *Pecten novaezelandiae* (JG/AMcI)	Wk7386	7760 ± 170	8183	7855–8552	1.7 ± 0.2	greenish black shelly sand, fining upward to shelly silty sand; core depth 40.5 cm
S1181	68	40°29.285′	175°06.313′	169	Shell - ^{14}C	oyster fragments (AB)	NZA17848 Wk12821	8286 ± 71	8815	8579–8955	1.8 ± 0.2	grayish olive green shell-rich silty sand, fining upward to sandy silt and silt; core depth 179 cm
S1182	74	40°31.212′	175°02.606′	70	Shell - ^{14}C	*Talochlamys gemmulata* (AB)	NZA178501 Wk12822	9244 ± 83	9835	9543–10286	1.2 ± 0.2	dark greenish grey shell-rich silty sand layer (8 cm thick), fining upward to sandy silt; core depth 148 cm
S1182	74	40°31.212′	175°02.606′	142–145	Wood - ^{14}C		Wk7489	12730 ± 290	14143	13446–15541	−27.7 ± 0.2	dark grey well-sorted sand with occasional pebbles and shells; core depth 148 cm
S1184	72	40°40.405′	174°59.464′	107	Shell - ^{14}C	*Austrofusus glans (AB)*	NZA178511 Wk12823	7815 ± 73	8281	8107–8394	1.6 ± 0.2	grayish olive green shelly silty sand, coarsening to shelly sand at base; core depth 135 cm
S1185	65	40°40.914′	175°0.459′	84-86	Wood - ^{14}C		Wk7488	9970 ± 250	10811	10125–11618	−26.3 ± 0.2	Grayish olive green pebbly, shelly silty sand, fining upward to sandy silt and grading downward to greenish black pebbly sand. Core depth: 110 cm
S1188	62	40°44.492′	174°58.241′	27	Shell - ^{14}C	Brachiopod (*Terebratella haurakiensis*) (DL)	NZA17843 Wk7487	7400 ± 72	7836	7678–7979	1.8 ± 0.2	Dark greenish grey shelly silty sand overlying 10 cm thick basal layer of large, well-rounded pebbles and shell fragments. Core depth: 55 cm

[a]The term ^{14}C indicates radiocarbon sample.
[b]Shell identifications for mollusks, JG/AMcI, J. Gillespie/A. McIntyre (Department of Earth Sciences, University of Waikato); AB, A. Beu (Institute of Geological and Nuclear Sciences (IGNS) Ltd, Wellington); for brachiopods, DL, D. Lee (University of Otago).
[c]Wk, University of Waikato, New Zealand; NZA, Accelerator Mass Spectrometer, IGNS Rafter Radiocarbon Laboratory, New Zealand.
[d]Conventional radiocarbon age calculated using a Libby half-life of 5568 a and corrected for isotopic fractionation. Quoted uncertainty is $\pm 1\sigma$.
[e]Calibrated age (2σ) in calendar years before present (A.D. 1950), based on *Stuivers and Reimer* [1993].

Table 2. Biostratigraphic Data From Selected Offshore Core Samples in the Kapiti-Manawatu Area

NIWA Station	Water Depth, m	Latitude South	Longitude East	Sample Depth, cm	Sediment Type	Biostratigraphic Interpretations		
						Age	Stage[a]	Paleoenvironment[b]
S1179	55	40°21.656′	175°07.995′	69–72	soft medium brown grey mud, Taupo pumice (1718 ± 30 calibrated a B.P.[b]) present?	late Pleistocene	tWq, ^{18}O stage 1	neritic (cool, northern) (diatoms, spicules)
S1180	71	40°29.123′	175°07.538′	90–93	soft medium grey fine silt, Taupo pumice present?	late Pleistocene	tWq, ^{18}O stage 1	paralic? (tepid, northern) (diatoms, sponge geodes and spicules, palynomorphs)
S1181	68	40°29.285′	175°06.313′	80–83	soft medium grey fine silt, Taupo pumice (1718 ± 30 calibrated a B.P.[b]) present?	late Pleistocene	tWq, ^{18}O stage 1	neritic (cool, northern) (diatoms, spicules)
S1181	68	40°29.285′	175°06.313′	165–168	soft medium grey shell and mud-rich sand	late Pleistocene	tWq, ^{18}O stage 1	neritic (cool, northern) (spicules, palynomorphs) (near maximum flooding surface?)
S1189	97	40°47.054′	174°52.280′	115–118	soft medium grey fine silt, Taupo Volcanic Zone volcanic glass present?	early Pleistocene	uWn	marine (reworked nannofossil, Oligo-E Mio) (diatoms, spicules)
S1190	95	40°46.358′	174°50.918′	65–68	soft medium grey silty sand	early-middle Pleistocene	mWc-mWq	neritic (tepid, southern) (diatoms, spicules, palynomorphs) (reworked nannofossil, Oligo-E Mio)
S1191	112	40°45.555′	174°49.414′	77–80	soft medium grey clay–rich silt	early–middle Pleistocene	Wc–mWq	neritic (tepid, northern) (diatoms, spicules, palynomorphs) (reworked nannofossil, Oligo–E Mio)
S1192	106	40°48.377′	174°50.526′	45–49	soft medium grey silty sand	early-middle Pleistocene	mWc	neritic (tepid, southern) (diatoms, spicules) (reworked nannofossil, Oligo-E Mio)
S1194	109	40°47.540′	174°48.874′	97–100	soft medium grey silt	early Pleistocene	tWn-lWc	neritic? (tepid, southern) (diatoms, spicules) (reworked nannofossil, Oligo-E Mio)
S1196	118	40°49.325′	174°46.253′	46–49	soft medium grey silt and shell-rich fine sand	Pleistocene	Wc-Wq, older than uWq	neritic (cool, southern) (diatoms, spicules) (reworked nannofossil, Oligo-E Mio)
S1197	116	40°55.108′	174°47.976′	30–33	soft medium grey fine silt	early Pleistocene	tWn-lWc	neritic (cool, southern) (diatoms, spicules) (reworked nannofossil, Oligo-E Mio)
S1197	116	40°55.108′	174°47.976′	80–83	soft medium grey clay	early Pleistocene	tWn-lWc	semineritic (tepid, southern) (diatoms, spicules, palynomorphs) (reworked nannofossil, E Mio)

[a]Wn, Nukumaruan; Wc, Castlecliffian; Wq, Haweran; l, lower; m, middle; t, top; u = upper; ^{18}O stage 1, deep ocean oxygen stage 1; Oligo, Oligocene; E Mio, early Miocene.
[b]Age of Taupo eruption tephra from *Alloway et al.* [2007].

Table 3. Summary of Neotectonic and Earthquake-Relevant Features of the Faults of the Offshore Kapiti-Manawatu Fault System for Fault Length, Area, Seafloor Scarp Height and Slip Rate[a]

Fault Name[b]	Fault Type[b]	Fault Zone[b]	Fault Length L,[c] km	Fault Area A,[d] km^2			Seafloor Scarp Height,[e] m			Slip Rate SR,[f] mm a^{-1}			
				Min	Average	Max	Min	Average (±1 SD)	Max	Min	Average	Max	120 ka
Kapiti	N	II	20.9	260.5	334.0	416.3				0.1	0.4	2.1	
Kapiti (total)	N	II	42.0	522.9	670.4	835.8	1.1	2.3 (1.4, n = 6)	4.5	0.1	0.4	2.1	0.7 ± 0.2
Mascarin (S)	R	II	33.4	416.3	533.8	665.4	2.3	2.9 (0.8, n = 5)	3.8				
Mascarin (N)	R	III	20.6	256.2	328.5	409.5	14.3	14.8 (2.2, n = 4)	18.0	0.1	0.6	0.2	
Mascarin (total)[g]	R	II-III	97.0	1207.7	1548.4	1930.3	2.3	7.6 (6.4, n = 10)	14.3	0.1	0.1	3.3	1.8 ± 0.5[g]
Okupe	R	I	6.0	74.7	95.8	119.4				0.5	0.6	1.5	
Okupe (total)	R	I	40.0	498.0	638.5	796.0	2.3	3.4	4.5	0.5	0.6	1.5	0.5 ± 0.2
Onepoto (S)	R	II	10.6	132.4	169.7	211.6	1.5	1.8 (0.4, n = 3)	2.3	0.0	0.1	0.1	1.3 ± 0.4
Onepoto (C)	R	II	3.3	40.6	52.0	64.8				0.1	0.6	1.5	
Onepoto (N)	R	III	22.6	281.8	361.3	450.5				0.4	0.6	1.5	
Onepoto (total)[g]	R	II-III	90.0	1120.6	1436.6	1791.0				0.2	0.4	1.0	
Otaheke (N)	R	III	16.3	202.8	260.0	324.2				0.9	1.0	1.2	
Otaheke (N) (total)	R	III	50.0	622.5	798.1	995.0				0.9	1.0	1.2	0.9 ± 0.3
Otaheke-Rangatira	N	I	4.3	53.4	68.4	85.3	4.5	11.0 (6.4, n = 3)	17.3	0.1	0.4	1.7	
Rangitikei	R	III	20.7	258.3	331.2	412.9				0.2	0.7	1.0	
Rangitikei (total)	R	III	45.0	560.3	718.3	895.5	3.8	11.9 (5.4, n = 5)	18.8	0.2	0.7	1.0	1.5 ± 0.4
Tangimoana	N	III	10.3	128.1	164.2	204.8							
Tangimoana (total)	N	III	13.0	161.9	207.5	258.7	23.3	27.8 (n = 2)	32.3				0.3 ± 0.1
Wairaka[h]	N	I	19.2	239.1	306.6	382.2	16.5	18.4 (n = 2)	20.3	0.2	0.4	0.5	0.2 ± 0.1
Waitarere (N)	R	II	16.6	207.1	265.5	331.0	1.5	4.6 (2.8, n = 11)	9.8	0.0	0.1	0.7	0.6 ± 0.2
Waitarere (S)	R	I	20.7	258.3	331.2	412.9	1.9	11.8 (8.7, n = 12)	30.0				
Waitarere (total)	R	I-II	55.0	684.8	877.9	1094.5				0.0	0.1	0.7	

[a]Slip rates are determined from offsets measured on the 10.8 ka post-last glacial erosion surface (PGS) and the seafloor, assuming a seafloor age of 6.5 ka (see text for details), and not from the seafloor scarp height only, as shown. Min, minimum; Max, maximum; SD, standard deviation; n, number of samples.

[b]Fault names and fault types are from Table 2 of *Lamarche et al.* [2005]. Fault zones I, II, and III are defined by this study (refer to text and Figure 2). Total, maximum subsurface length of the fault from *Lamarche et al.* [2005]; N, northern section; C, central section; S, southern section; N, normal fault; R, reverse fault.

[c]Fault lengths are derived from field measurements based on the distribution of seafloor scarps (this study, see Figure 2). The total subsurface length for Wairaka, Onepoto (S), Mascarin, Otaheke (N), and Rangitikei faults includes onshore sections, as described by *Lamarche et al.* [2005].

[d]Estimates of fault areas are derived by calculation from the various values of length and width of the fault assuming a maximum fault dip of 70° [*Lamarche et al.*, 2005] and a preferred seismogenic depth of 15 ± 2 km for the KMFS faults based on historical seismicity data [*Stern et al.*, 1992; *Reyners*, 1998]. Minimum and maximum seismogenic depths are estimated to be 13 and 17 km, respectively (i.e., 15 ± 2 km), and have been used in the calculations of minimum and maximum fault area.

[e]Minimum, average, and maximum seafloor scarp heights for the fault (based on field mapping results, Figure 2). These seafloor scarp heights are not used in the subsequent calculation of fault slip rates due to uncertainties associated with the age of the seafloor, which is inferred to be 6.5 ka, but at certain locations on the continental shelf could either be older or younger than this estimate (see text for details and footnote f).

[f]Minimum, average, and maximum annual slip rates of the fault based on field mapping and interpretation of deformation of the 10.8 ka post-last glacial erosion surface (PGS, Table 1). This calculation also accounts for the inferred age of the seafloor (6.5 ka), and therefore includes an element of uncertainty, but nonetheless offers a more robust estimate of actual fault slip rates than provided by using seafloor scarp offsets directly (see text for details and note e). The slip rates for each fault, shown here as minimum, average, and maximum values, are taken from all measurements that were made along the fault. In locations where deformation has occurred on the nearshore sediment wedge (Figure 2) and where the age of the seafloor may be less than 6.5 ka, slip rates should be regarded as minimum values. Here 120 ka indicates the maximum slip rate over the last 120 ka period from Table 3 of *Lamarche et al.* [2005], assuming a fault dip of 70°For all faults, except for Rangitikei and Wairaka faults, where a dip of 80° was used. Note that an older age of 260 ka has also been proposed, but not confirmed, for the H1 horizon [*Lamarche et al.*, 2005; *Proust et al.*, 2005]. The ±30% error estimates given for the 120 ka slip rate takes into account fault dips of 65–75°. The Wairaka 120 ka slip rate is for its northern section only.

[g]Calculations made assuming no segmentation along Onepoto and Mascarin faults [*Lamarche et al.*, 2005], except that average slip rates for the Mascarin Fault can only be estimated for the northern section.

[h]For northern offshore sections of the Okupe and Wairaka faults only, except for the fault length of Okupe (total), which is for the entire subsurface extent of the fault.

and its dip (Table 3). Seismogenic depth is related to the distribution of historical crustal seismicity in the WB [e.g., *Stern et al.*, 1992; *Reyners*, 1998] and was estimated to be about 10–15 km based on the distribution of crustal seismic activity in the study area [*Stern et al.*, 1992]. Below these depths is a region of concentrated seismicity that defines the inclined subduction interface between the overlying Australian Plate and the subducting Pacific Plate at 40–50 km depth [*Robinson*, 1986; *Stern et al.*, 1992; *Ansell and Bannister*, 1996; *Reyners*, 1998]. These observations suggest that faulting within the KMFS is probably seismogenic and for some of the larger structures may be linked to the subduction interface [*Lamarche et al.*, 2005]. In this study, a conservative estimate for the seismogenic depth of 15 ± 2 km was assumed.

3.4. Estimation of Earthquake Source Parameters

[21] Potential earthquake moment magnitudes (M_w) were estimated using empirical relationships based on measured or estimated fault parameters: fault rupture length (L), area (A) and width (W), assuming fault dips of 70° and a range of seismogenic depths (i.e., 15 ± 2 km, see above). For normal and reverse faults, the following empirical equations were used:

$$M_w = 3.39 + 4/3 \log_{10}(A) \quad (1)$$

for normal faults [*Villamor et al.*, 2001], and

$$M_w = 4.18 + \log_{10}(L) + \log_{10}(W) \quad (2)$$

for reverse faults [*Berryman et al.*, 2002]. These new fault scaling relations for New Zealand fault sources were developed due to the recognition that such scaling is dependent on the aspect ratio between rupture length and rupture width, which in many New Zealand examples are actually width limited (i.e., rupture length generally exceeds rupture width) [*Berryman et al.*, 2002]. The new relations account for this observation and also comply with existing seismological and geological data. This is especially important for normal-slip faults where previous scaling relations between rupture length and seismic moment, derived mainly from extensional faults in the Taupo Volcanic Zone, were found not to be widely applicable to other similar fault sources outside this region [*Villamor et al.*, 2001].

[22] As mentioned previously, maximum and minimum fault areas were calculated from the estimated range of seismogenic depths (13–17 km), although 15 km is the preferred depth. The designations of "minimum", "preferred" and "maximum" flow though subsequent calculations of M_w, seismic moment (M_o), single-event displacement (SED) and recurrence interval (RI). From the M_w calculations for each fault source based on minimum, preferred and maximum fault area, M_o estimates were derived from

$$\log_{10}(M_o) = 16.05 + 1.5M_w, \quad (3)$$

where M_o is in units of dyn cm [*Hanks and Kanamori*, 1979]. From these values, the minimum, preferred and maximum SEDs were estimated using *Aki and Richards*' [1980] equation:

$$M_o = \mu A(SED), \quad (4)$$

where μ is rigidity modulus (3×10^{11} dyn cm [*Brune*, 1968]).

[23] Slip rates (SR) were approximated using the measured vertical offsets and inferred ages of the seafloor and the buried PGS reflector. In order to derive a robust estimate of fault SR, an assumed seafloor age of 6500 a was used, which is approximately the time that sea level reached its present position following the post-last glacial transgression [*Carter et al.*, 1986; *Gibb*, 1986] (see discussion below). Close to the coast, however, the development of a nearshore sediment wedge that has formed since sea level stabilized at 6500 a ago (Figure 2) means that this estimated age of the seafloor is conservative. It is recognized that on the inner shallow parts of the wedge, which were not largely surveyed by this study, the surficial sediments could be younger than 6500 a old due to late Holocene riverine sediment inputs and longshore drift and other coastal processes. There are no data with which to constrain the actual age of the seafloor in such environments and the assumed age of 6500 a is a reasonable estimate based on knowledge of post-last glacial sea level rise around New Zealand [*Carter et al.*, 1986; *Gibb*, 1986]. Minimum, average and maximum slip rates were calculated from all locations where such measurements could be made from the geophysical profiles that intersected the fault traces. In this regard, SR estimates, as presented in Table 3, are best regarded as conservative since they are calculated from the offset and timing differences between the seafloor and the 10.8 ka buried PGS reflector, and not from the seafloor offsets alone. This more prudent approach is best applied where the mapped nearshore wedge has been deformed by faulting on underlying structures of the KMFS (Figure 2). In these cases, there are issues with the inferred age of the seafloor and the likelihood that high seafloor scarps do not represent discrete, single-event displacements (see text below).

[24] The SR and estimated single-event displacement data were then used to determine the minimum, average and maximum RIs for the faults where

$$RI = SED/SR. \quad (5)$$

[25] For many cases in the KMFS, SED may be approximated by the height of the seafloor scarp (D), especially where D is less than 5 m. Since single-event displacements for onshore strike-slip faults in southern North Island are in the order of 3–5 m [*van Dissen and Berryman*, 1996; *Heron et al.*, 1998; *Litchfield et al.*, 2004], as also inferred for dip-slip faults elsewhere in the region [e.g., *Nodder*, 1994; *Nicol et al.*, 2005], it is possible that scarps on offshore faults in the KMFS that are <5 m in height could be single-event structures, or alternatively could represent many moderately sized earthquakes. In other examples, where seafloor scarps are much greater than 5 m (e.g., Wairaka Fault, Tangimoana Fault), it is probable that multiple displacement events have occurred. In such cases where seafloor scarps are >5 m in height, estimated recurrence intervals for a given slip rate will be overestimated. At some locations in the study area, such as west of Kapiti Island, this is likely to be compounded further by poor age control of the deformed strata (e.g., southern sections of the Waitarere Fault where undifferentiated Plio-Pleistocene sediments are deformed by near-surface faulting) (see later).

[26] For comparison, we also estimated M_w using other empirical equations utilizing seismic moment and fault area estimates (derived from calculations above), and fault seafloor rupture lengths and slip rates from field measurements, as in Figure 2 and Tables 3 and 4 [e.g., *Hanks and Kanamori*, 1979; *Wells and Coppersmith*, 1994; *Anderson et al.*, 1996; *Stirling et al.*, 2002a, 2002b]. Many of these empirical methods have been developed essentially from and applied to normal fault systems, although *Barnes et al.* [2002] undertook an earthquake recurrence analysis on the Lachlan Thrust Fault in the offshore forearc environment of the Hikurangi subduction system in Hawkes Bay, New Zealand. Here, we apply similar techniques for the first time to the reactivated reverse faults of the KMFS in the back-arc environment of the same subduction margin.

3.5. Errors in Horizon Definition From Seismic Reflection Data

[27] Errors on horizon depth in two-way traveltime interpreted on the 3.5 kHz profiles are estimated to be ±0.25 ms (i.e., ~20 cm at 1600 m s^{-1}). Errors on the velocities used for depth conversions of MCS data are given by the standard deviations from the mean calculations, and are approximately 5–10% at shallow depths [*Lamarche et al.*, 2005]. The largest uncertainty on displacement measurements arise from asymmetric fault drag adjacent to fault planes observed in foot walls and hanging walls and across seafloor scarps. *Lamarche et al.* [2005] estimated an overall relative error of ±30% for the slip rates derived from MCS

Table 4. Earthquake Parameters of Moment Magnitude M_w, Seismic Moment M_o, Single-Event Displacement, and Recurrence Interval for the Faults of the Offshore Kapiti-Manawatu Fault System[a]

	Moment Magnitude M_w[c]			Seismic Moment M_o,[d] $\times 10^{25}$ dyn cm			Single-Event Displacement SED,[e] m			Recurrence Interval (RI, years)[f]		
Fault Name[b]	Min	Mw	Max	Min	M_o	Max	Min	SED	Max	Min	RI	Max
Kapiti	6.6	6.7	6.9	9.0	14.8	22.9	0.8	1.3	1.8	402	3068	33074
Kapiti (total)	7.0	7.1	7.3	36.2	59.4	92.2	1.7	2.6	3.7	804	6137	66168
Mascarin (S)	6.8	6.9	7.0	17.7	25.8	35.9	1.0	1.4	1.8	314	23259	29850
Mascarin (N)	6.6	6.7	6.8	8.6	12.4	17.3	0.8	1.1	1.4	5310	1834	23416
Mascarin (total)[g]	7.3	7.4	7.5	87.7	127.3	177.2	1.7	2.4	3.1	535	39614	50840
Okupe[h,i]	6.1	6.2	6.3	1.4	2.0	2.7	0.4	0.6	0.8	285	1041	1430
Okupe (total)	6.9	7.0	7.1	23.2	33.7	46.9	1.1	1.5	2.0	735	2689	3691
Onepoto (S)[i]	6.3	6.4	6.5	3.2	4.6	6.4	0.6	0.8	1.0	6923	14449	109404
Onepoto (C)[i]	5.8	5.9	6.0	0.5	0.8	1.1	0.3	0.4	0.6	216	781	5047
Onepoto (N)	6.6	6.7	6.8	9.9	14.3	20.0	0.8	1.2	1.5	568	2058	3991
Onepoto (total)	7.2	7.3	7.4	78.4	113.8	158.4	1.7	2.3	2.9	1653	5869	18018
Otaheke (N)	6.5	6.6	6.7	6.0	8.8	12.2	0.7	1.0	1.3	603	942	1411
Otaheke (N) (total)	7.0	7.1	7.2	32.5	47.1	65.6	1.3	1.7	2.2	1056	1651	2471
Otaheke-Rangatira[i]	5.7	5.8	6.0	0.4	0.6	1.0	0.2	0.3	0.4	103	623	3564
Rangitikei	6.6	6.7	6.8	8.7	12.6	17.5	0.8	1.1	1.4	779	1614	6504
Rangitikei (total)	6.9	7.0	7.1	27.7	40.2	56.0	1.2	1.6	2.1	1147	2377	9578
Tangimoana[i]	6.2	6.3	6.5	2.2	3.6	5.6	0.4	0.6	0.9			
Tangimoana (total)[i]	6.3	6.5	6.6	3.5	5.7	8.9	0.5	0.8	1.1			
Wairaka[h]	6.6	6.7	6.8	7.6	12.5	19.3	0.8	1.2	1.7	1470	3316	7594
Waitarere (N)	6.5	6.6	6.7	6.2	9.0	12.6	0.7	1.0	1.3	1089	9805	91229
Waitarere (S)	6.6	6.7	6.8	8.7	12.6	17.5	0.8	1.1	1.4			
Waitarere (total)	7.0	7.1	7.2	37.4	54.4	75.7	1.3	1.8	2.3	1980	17829	165890

[a]SED, single-event displacement; RI, recurrence interval. Definitions and abbreviations are as in Table 3 (this study).

[b]Fault names are from Table 2 of *Lamarche et al.* [2005].

[c]Minimum, preferred, and maximum values of the earthquake moment magnitude expected to accompany rupture of the fault. All values are calculated from the equations: $M_w = 3.39 + 1/33\log_{10}A$ for normal faults [*Villamor et al.*, 2001] and $M_w = 4.18 + 2/3\log_{10}W + 4/3\log_{10}L$ for reverse and reverse-oblique faults [*Berryman et al.*, 2002] where A is fault area, W is fault width based on fault length (L) and assuming a fault dip of 70° (Table 3).

[d]Minimum, preferred, and maximum values of seismic moment based on estimated earthquake moment magnitude, where $\log_{10}(M_o) = 16.05 + 1.5M_w$ [*Hanks and Kanamori*, 1979].

[e]Minimum, preferred, and maximum values of the single-event displacement for the fault with scaling factors to relate subsurface to surface displacement. SED is derived from the equation of *Aki and Richards* [1980]: $Mo = \mu A(SED)$, where μ is rigidity modulus (3×10^{11} dyn cm [*Brune*, 1968]), A is fault area, and SED is single-event displacement. Note 10^5 cm = 1 km. For minimum, preferred, and maximum SED the scaling factors are 0.7, 0.8, and 1.0, respectively, i.e., between 70% and 100% of the displacement at depth is registered at the ground surface [*Villamor et al.*, 2001; *Berryman et al.*, 2002; *Stirling et al.*, 2002b].

[f]Minimum, preferred, and maximum values of recurrence interval (RI), in years between earthquake events. The values are derived by dividing the various values of SED by the slip rate (Table 3) where RI = D/SR.

[g]Assuming no segmentation along the fault [e.g., *Lamarche et al.*, 2005].

[h]For northern offshore sections of the Okupe and Wairaka faults only, except for the fault length of Okupe (total), which is for the entire subsurface extent of the fault.

[i]Fault lengths (Table 3) are shorter than the assumed seismogenic depth of 15 km, as supported by seismological and other geological data from the region [*Smith*, 1979; *Garrick and Gibowicz*, 1983; *Townsend*, 1998] (also see note d in Table 3) and hence result in an unrealistic shape ratio (L/15) of <1 for these fault sources. These data are included here for completeness but have been excluded from further analyses of the earthquake source data, as presented in the text.

data, representing the sum of the relative errors associated with sound velocity estimates (5%), displacement measurements (15%) and reflector age estimates (15%). The errors for displacement measurements made on high-resolution geophysical data (3.5 kHz and Uniboom) are estimated to be ~5%, while those on the age of the PGS from radiocarbon dating are 7% (Table 1), yielding a total relative error on the slip rate derived from the high-resolution data of ±12%.

4. Results

4.1. Late Quaternary Stratigraphy of Offshore Kapiti-Manawatu

4.1.1. The 3.5 kHz and Uniboom Data

[28] There is a pronounced break in slope approximately 7–10 km offshore at water depths of 60–70 m (gradient of 1:100 to 1:170, <1°), representing the modern-day nearshore sediment wedge deposited westward from the present coastline along the Kapiti-Manawatu coast [e.g., *Dunbar and Barrett*, 2005] (Figures 2 and 5). Here, a moderately strong, inclined planar reflector within the wedge (reflector A) laps onto a regular, subhorizontal opaque reflector (reflector B), corresponding to the post-last glacial erosion surface (PGS) (see later). Near the base of the nearshore sediment wedge, reflector A is truncated at the seafloor while reflector B becomes more subparallel with an overlying, semiopaque upper unit, thickening westward from <5 to 15 ms (Figure 5). Beneath reflector B, subsurface reflectors are inclined, chaotic and/or truncated. Gas masking of sediments occurs at shallow sediment depths on the inshore upper part of the modern wedge (Figures 2 and 5a). The upper surface of the wedge is also locally deformed by faults (Figures 5 and 6).

[29] To the west of the nearshore wedge, the uppermost semiopaque layer above reflector B becomes progressively

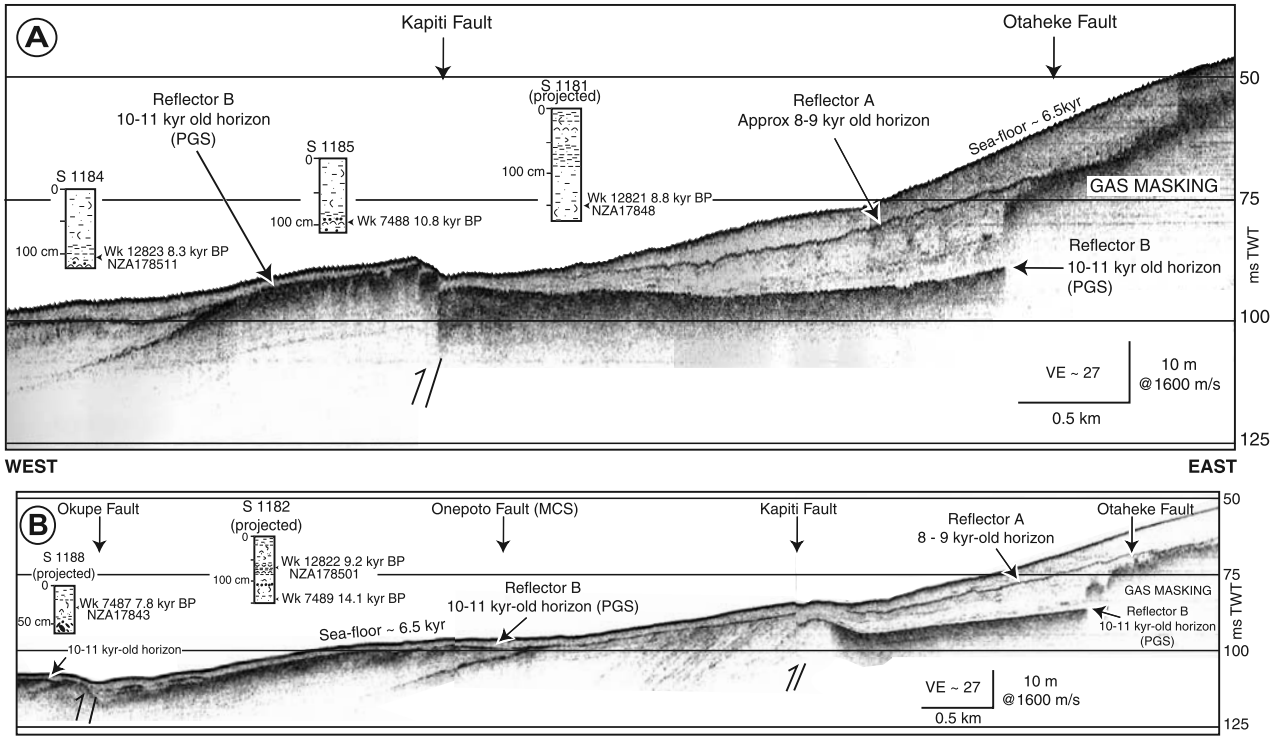

Figure 5. Deformation at the foot of the nearshore sediment wedge, showing active faults, inferred ages of seismic reflectors and core logs. (a) The 3.5 kHz profile CR3048-line 29. (b) CR3048-line 62. PGS is the post-last glacial erosion surface associated with the last marine transgression between 20 and 6.5 ka. The diachronous age of the PGS as dated at specific core locations is indicated. (MCS) indicates that faults are identified on MCS profiles only and have no surface expression (e.g., Onepoto Fault). Faults are indicated with a bold line with the sense of movement, as interpreted from MCS profiles, indicated with a half arrow. Profile locations are shown on Figure 2.

buried (up to 15 ms deep) and more transparent in character (Figure 5b). This layer overlies buried sand ridges on the inner continental shelf, which are opaque units with a smoothly undulating, strong reflector at their upper surface [e.g., *Gillespie et al.*, 1998].

[30] Packets of unconformity bound units, comprising numerous subparallel, inclined reflectors, are interspersed between basement features and are commonly truncated at the seafloor, especially west of Kapiti Island (Figure 7). Seismic penetration was generally good in these areas (often

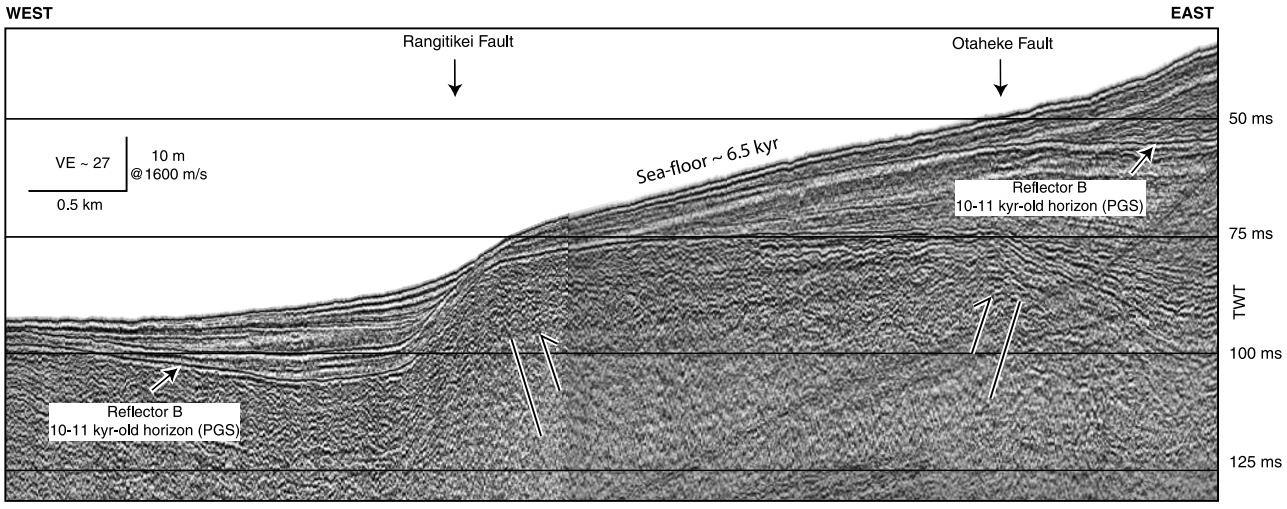

Figure 6. Uniboom profile across northern part of the nearshore sediment wedge; TAN0105-line B20. Profile location is shown on Figure 2.

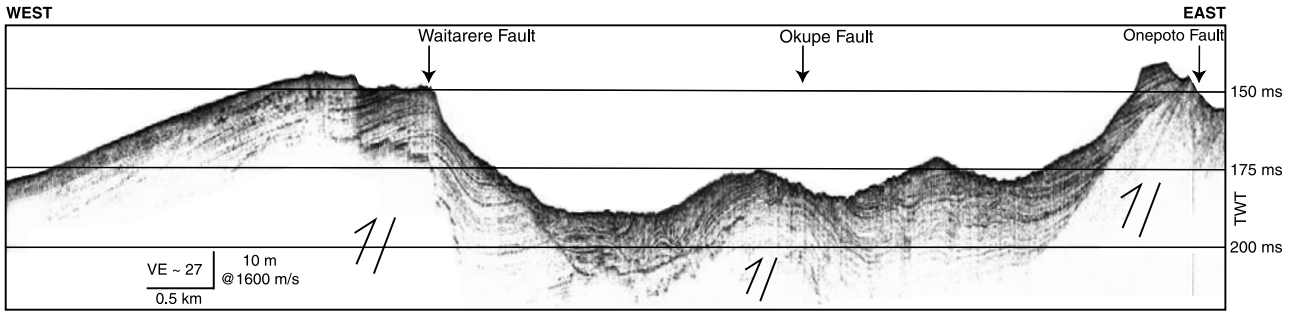

Figure 7. High seafloor scarps in semiconsolidated Plio-Pleistocene sedimentary rocks in zone I of the KMFS, northwest of Kapiti Island; 3.5 kHz profile CR3048-line 65. Profile location is shown on Figure 2.

>25 ms). These units represent Plio-Pleistocene sediments [e.g., *Lewis et al.*, 1994] that at certain localities lie on irregular unconformities, commonly marking the upper surface of underlying acoustically opaque basement rocks. In addition, on the seaward side of the Mascarin Fault, which is marked by a bathymetric break-in-slope on the inner shelf at water depths of 40–80 m, a thickening wedge of possibly mainly post-last glacial sediment with vertical stacking of several channel sequences is also apparent (Figure 3d).

4.1.2. Core Data

[31] Suitable shells and wood for radiocarbon dating were obtained from sedimentary units overlying or corresponding to seismic reflectors identified in 3.5 kHz records (Table 1 and Figure 5). Core analysis suggests that the post-last glacial erosion surface (reflector B or PGS), is characterized lithologically by large angular shell fragments (mainly shallow water bivalves, *Pecten novaezelandiae*, *Talochlamys gemmulata*, oyster fragments) and occasional well-rounded pebbles in a silty sand matrix (Table 1 and Figure 5). The coarse-grained layer is underlain by moderately well sorted, fine-medium gravelly and shelly silty sands and overlain by grey olive-green sandy silts with small, subangular shell fragments. The uppermost sandy silts represent recent deposits, dated as late Haweran (oxygen isotope stage 1) using nannobiostratigraphy (Table 2). Compact, grey-green to blue-grey silty deposits, corresponding to the well-bedded packages of subsurface reflectors west and south of Kapiti Island (Figure 7), are dated generally as early to middle Pleistocene in age (New Zealand stages upper Nukumaruan to lower Castlecliffian), and contain numerous reworked Oligocene to early Miocene nannoflora (Table 2), as documented previously in the region by *Lewis et al.* [1994].

[32] The strong near-surface reflector B (PGS) represents a lag deposit associated with the erosional hiatus caused by the post-last glacial marine transgression, and has an average ^{14}C age of ~10 800 calendar (cal) years B.P. (range: 10,125–11,618 cal years B.P., 2 standard deviations) (Lab sample Wk7488, Table 1). The interpretation is supported by an independent estimate of the rate of the post-last glacial marine transgression across the Taranaki-Wanganui shelf. The 10–11 ka transgressive ravinement surface is located at ~70 m below present sea level off the Manawatu coast (Figure 5a) and the equivalent reflector, dated at 14–15 ka on the outer Taranaki shelf, occurs at 119 m below sea level (sample Wk1890 [*Nodder*, 1994]). These data suggest that sea level transgressed at an average rate of ~12 mm a^{-1} across the Taranaki-Wanganui shelf, which agrees reasonably well with *Carter et al.*'s [1986] "SW Pacific" rate of 8–10 mm a^{-1}, especially if the WB has also subsided at a rate of 1–2 mm a^{-1} over this time period [e.g., *Anderton*, 1981; *Norris and Grant-Taylor*, 1989; *Proust et al.*, 2005]. Therefore an age of 10.8 ka was adopted for the PGS in the coastal region of the Wanganui Basin, and used in subsequent determination of earthquake source parameters, such as fault slip rates.

4.2. Seafloor Scarps and Near-Surface Deformation

[33] Seafloor scarps and near-surface deformation are observed for most of the main structures within the KMFS (Figure 2 and Figures 5–10). Mainly on the basis of the distribution of seafloor scarps, three major zones of recent deformation occur within the offshore KMFS: (1) zone I around Kapiti Island is characterized by the development of large, often eroded seafloor scarps (~10–30 m high) on the Waitarere, Okupe, Otaheke, Rangatira and Wairaka faults; (2) zone II by moderate scarp development (~1–5 m high) on the Kapiti and northern section of the Waitarere Fault and minor seafloor offsets on the Onepoto, Okupe and Mascarin faults; and (3) zone III by prominent bathymetric changes in seafloor slope (>10 m high) that are possibly surface expressions of the Mascarin, Onepoto, Rangitikei, Otaheke and Tangimoana faults (Figure 2). Zone II may be further subdivided into an offshore subzone where deformation is dominated by the Waitarere and Mascarin faults and an inshore zone in the southern part of zone II characterized by smaller scarps (1–3 m high) on the Kapiti, Onepoto and Okupe faults. Neotectonic deformation characteristics in each of the three main zones are considered in detail below.

4.2.1. Zone I: Kapiti Island

[34] The highest seafloor scarps in the KMFS are located immediately north and west of Kapiti Island on 5–12 km long sections of the Waitarere and Otaheke/Rangatira faults (Figure 2). West of Kapiti Island, seafloor elevations of 25–30 m and 15 m are observed in eroded Plio-Pleistocene sediments along the Waitarere and Okupe faults over distances of 17 and 5–6 km, respectively (Figure 7). These estimates represent minimum values due to extensive erosion of the seafloor at these localities. East of Kapiti Island in Rauoterangi Channel, it is difficult to determine whether the prominent 15–22 m high bathymetric slopes that define the western and eastern sides of the channel are related to

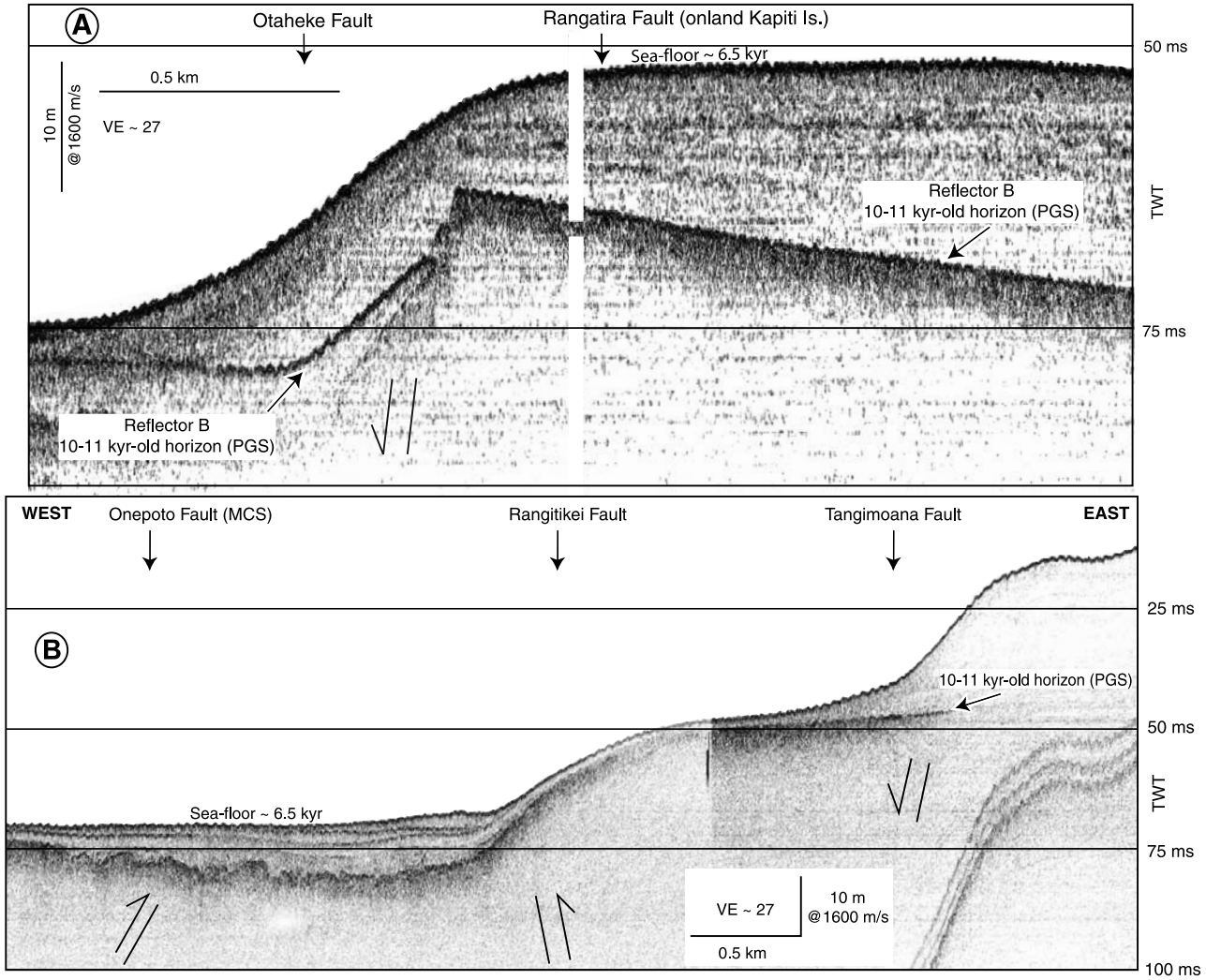

Figure 8. Influence of near-surface deformation on nearshore bathymetric features. (a) Subsurface faulting and channel margin development in the Rauoterangi Channel between Kapiti Island and the coast. 3.5 kHz profile CR3048-line 32. (b) Steep bathymetric slopes off Manawatu river mouth. (MCS) indicates that faults are identified on MCS profiles only and have no surface expression; 3.5 kHz profile TAN0105-line 24. Profile locations are shown on Figure 2.

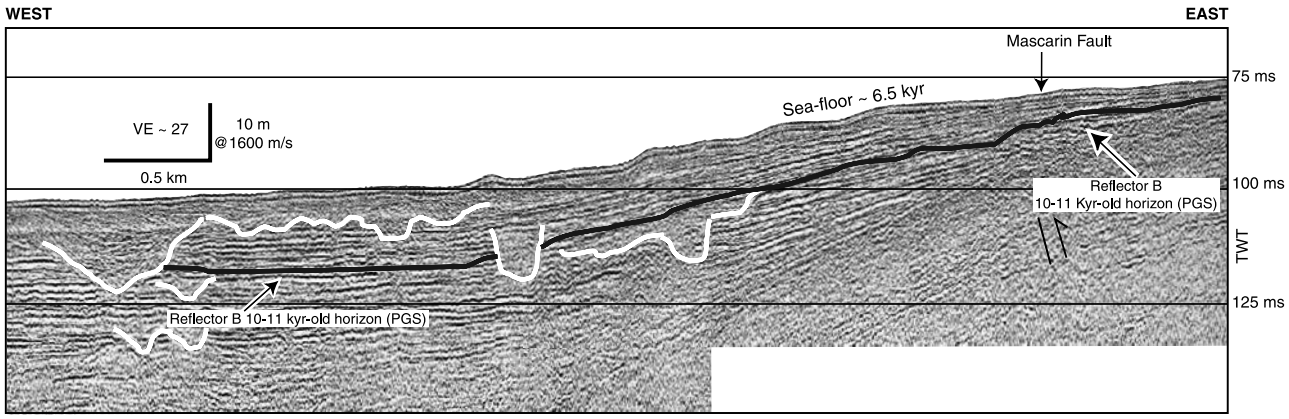

Figure 9. Broad seafloor "scarp" and synsedimentary thickening of subsurface reflectors associated with Mascarin Fault deformation. White lines indicate paleochannels formed either during the last glacial lowstand in sea level or stillstands during the subsequent transgression; Uniboom profile TAN0105-B15. Profile location is shown on Figure 2.

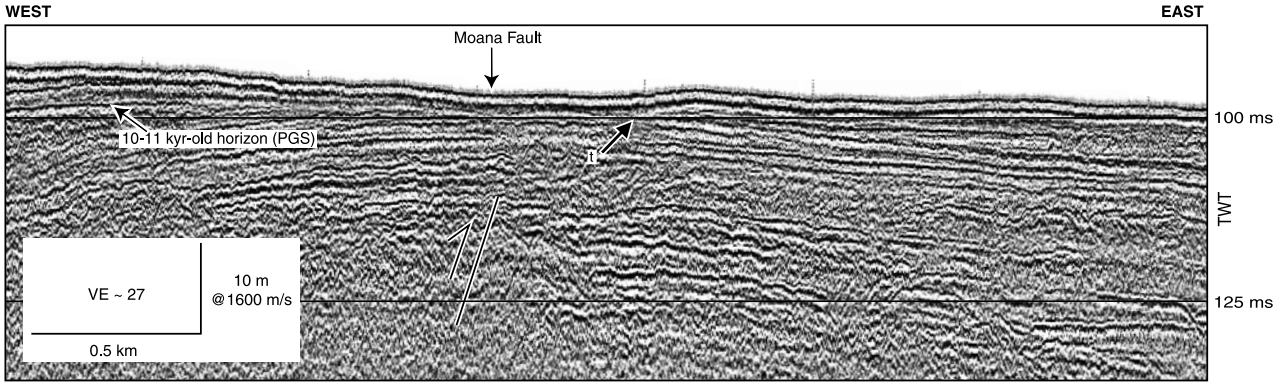

Figure 10. Truncated anticline associated with Moana Fault deformation; Uniboom profile TAN0105-B20. Truncated reflectors (t) are indicated by the solid arrow. Profile location is shown on Figure 2.

faulting activity. Certainly, traces of the Otaheke/Rangatira and Wairaka faults underlie the channel flanks and deformation of near-surface reflectors is recognized from shallow seismic reflection profiles (Figure 8a). These observations indicate that channel morphology is probably controlled structurally by late Quaternary deformation. If this is the case then the Otaheke Fault may have near-surface expression over a distance of 20–30 km with significant bathymetric relief along its entire length. In comparison, while subsurface deformation on the Wairaka Fault suggests a maximum fault length of 16–17 km, there is significant bathymetric expression of this recent activity only over a central 3 km long section of the fault (Figure 2).

[35] Late Quaternary slip rates in zone I range from 0.1 mm a^{-1} to a maximum of 1.7 mm a^{-1} on the Otaheke/Rangatira fault trace north of Kapiti Island. The high slip rate estimates of >1.5 mm a^{-1} for certain sections of the faults in zone I (e.g., Otaheke/Rangatira and Okupe faults) and lack of slip rate data for others reflect difficulties in correlating reflectors between geophysical lines due to poor seismic penetration at shallow water depths (e.g., Otaheke/Rangatira and Wairaka faults) and limited age control of deformed, near-surface reflectors (e.g., eroded southern sections of Waitarere and Okupe faults). Slip rates in this zone are typically low (<0.4 mm a^{-1}), and associated with high surface displacements, characterized by often eroded, 10–30 m high seafloor scarps, and with variable seismic moment estimates ($\sim 1-50 \times 10^{25}$ dyn cm) (Table 3).

4.2.2. Zone II: Kapiti Island to Manawatu River

[36] Between Kapiti Island and the mouth of the Manawatu River, prominent seafloor scarps up to 10–11 m in height are identified along the northern part of the Waitarere Fault (Figure 2). Lower offsets are observed on the Kapiti and the southern part of the Onepoto Fault, with scarp heights of 3–5 and 1–2 m, respectively. As surface relief on the Kapiti Fault diminishes to the north, deformation appears to be taken up on the 17 km long northern section of the Waitarere Fault and perhaps on the Mascarin Fault further to the west. In addition, a localized, 2–6 km long strand of the Okupe Fault appears to accommodate a portion of the near-surface deformation between the southern and northern sections of the Waitarere Fault, as evinced by a pronounced seafloor scarp between 2 and 4 m in height (Figures 2 and 5b). Northeast of here, the Kapiti Fault is recognized by a nearly continuous, linear seafloor scarp that is formed along and deforms locally the base of the modern nearshore sediment wedge (Figure 5).

[37] A small, 1–2 m high, very localized scarp on the Onepoto Fault occurs immediately west of the surface trace of the Kapiti Fault where seafloor relief on the latter seems to be subdued, although significant deformation (up to 8 m vertical offset) of the near-surface 10.8 ka post-last glacial reflector is apparent (Figure 2). Seaward of the modern nearshore sediment wedge, subsurface deformation of the 10.8 ka post-last glacial surface is observed along the Onepoto Fault. Vertical offsets of 1–5 m, rising to 14–16 m at the northern end of the fault trace, are found on this reflector, but this deformation is not associated with a seafloor scarp (Figure 5b). Similarly, subsurface offsets of 5 and 10–13 m on the PGS are observed on short sections of the Otaheke and Moana faults, respectively, without associated deformation of the seafloor (Figure 6).

[38] Slip rates on these faults are generally low to very low (<0.2 mm a^{-1}) with small seismic moment estimates (<15×10^{25} dyn cm), except on the entire Kapiti Fault with M_o estimates has high as 90×10^{25} dyn cm (Table 3). A maximum slip rate of 2.1 mm a^{-1} was calculated on the Kapiti Fault, compared to an average slip rate estimated from several locations along the fault of 0.4 ± 0.3 mm a^{-1}.

4.2.3. Zone III: Mascarin Fault and Deformation of the Nearshore Sediment Wedge

[39] The Mascarin Fault is recognized by *Lamarche et al.* [2005] as the westernmost and largest fault within the KMFS. From seafloor and subsurface profiles, a marked break in the regional bathymetric slope in the north of the study area is interpreted as a seafloor flexure controlled by the underlying Mascarin Fault (Figures 2 and 3a). Here, seafloor height offsets of 9–15 m over a lateral extent of 17–21 km are observed and a substantial wedge of last-post glacial sediment has accumulated on the downthrown side of the fault and effectively smothered its active seafloor trace (Figures 3d and 9). Small, localized seafloor scarps (2–3 m in height) associated with splays from the main Mascarin Fault trace (Ma2 and Ma3) are also present close to the coastline in the north (Figure 2). Between 40 and 65 km along the Mascarin Fault, seafloor scarps of 2–4 m are observed, although, since the low-relief scarp front is parallel to regional bathymetric contours and there is poor

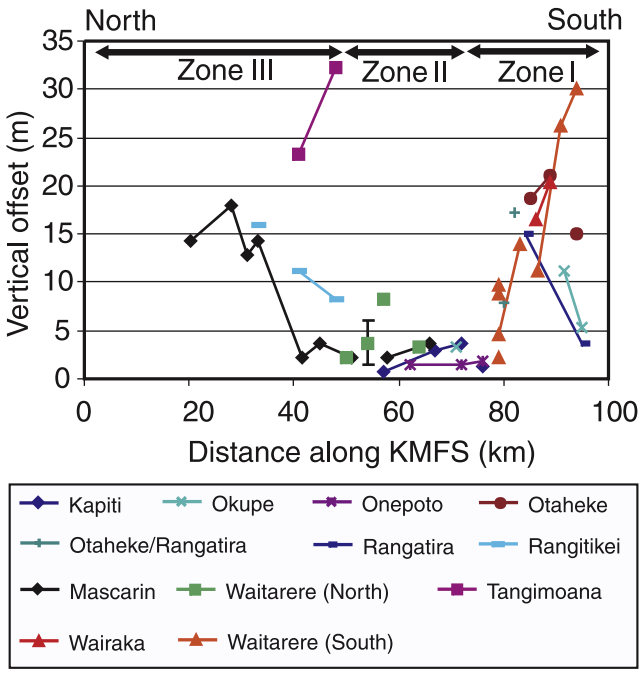

Figure 11. Vertical offset of the seafloor (in meters) and projected distance (in kilometers) along all faults of the KMFS based on the surface deformation map (Figure 2). Estimated errors in vertical offsets are shown as error bars (±1 standard deviation). The N23°E projection axis origin is located along the Wanganui coast at the mouth of the Whangaehu River at the northern end of the KMFS (refer Figure 2).

resolution of seismic profiles at these shallow water depths, it is difficult to make an unambiguous conclusion that there is a continuous seafloor scarp. If the scarp is continuous along the Mascarin Fault, the fault would have a maximum seafloor rupture length of 54 km (Table 3). On the contrary, if there is no scarp continuity across seismic lines, the fault length could be as low as 10–12 km (Figure 2), but this is unlikely given the unambiguous continuous nature of the structure from MCS data [*Lamarche et al.*, 2005]. South of 40°35′S, the Mascarin Fault essentially becomes a basement feature, with active deformation occurring on other structures to the east of the fault near Kapiti Island (see below).

[40] Inshore of the Kapiti Fault, a pronounced change in the bathymetric slope halfway up the nearshore sediment wedge is located above the Otaheke Fault, as imaged on MCS profiles. It is not obvious, however, that near-surface horizons have been displaced due to pervasive gas masking within the wedge. This zone of gas masking extends over a distance of 22 km across the inferred boundary between zones II and III (Figure 2), where it is associated with small breaks in the slope, which probably represent the near-surface location of the Otaheke Fault, as confirmed by MCS data (Figure 5a). The gas masking stops where the break in slope bifurcates northward into two distinct areas of steeper slope on the upper surface of the sediment wedge between Manawatu and Rangitikei rivers (Figure 2).

[41] From just south of the Manawatu River northward to the Rangitikei River mouth, two contiguous zones of steep bathymetric relief on the westward dipping surface of the nearshore sediment wedge correspond to the seafloor expressions of the Rangitikei and Tangimoana faults (Figures 2 and 8b). Steeply dipping reflectors, associated with the Tangimoana Fault, are exposed at the seafloor atop a prominent 23–32 m high slope over a lateral distance of about 10 km. West of the Tangimoana Fault and along the toe of the nearshore sediment wedge, the 11–19 m high slope, representing the surface expression of the Rangitikei Fault, is associated with vertical offsets on the 10.8 ka reflector in the order of 10–23 m. These subsurface offsets remain high, even as the slope/scarp height decreases progressively to the north (Figure 2). The Rangitikei Fault may have surface expression over a distance of about 21 km, assuming continuity between these zones of substantial offset and bathymetric relief, but alternatively could be broken up into several, less extensive segments ranging in length from 3 to 7 km.

[42] To summarize, zone III is dominated by fault structures that have high surface offsets (~10–30 m), moderate to high slip rates (>0.1–3.0 mm a^{-1}) and high seismic moment potential (up to maximums of 160–180 × 10^{25} dyn cm (Table 3). In some cases, correlation of reflectors between seismic lines was hampered by difficulties in imaging subsurface reflectors due to the rough sea state during surveying (e.g., Mascarin, Rangitikei and Onepoto faults). Nonetheless, in general, it appears that faults in zone III represent the most active structures in the KMFS.

5. Discussion

5.1. Styles of Neotectonic Deformation

[43] Spatial patterns of deformation within the offshore KMFS indicate that the highest levels of neotectonic deformation are concentrated in the south and north of the study area (zones I and III, respectively) (Figures 11 and 12). In zone I, the vertical offset estimates are also likely to be minimum values due to considerable seafloor erosion, related to strong tidal current scour in the northern part of Cook Strait [*Carter*, 1992]. In addition, it is difficult to trace these structures south of Kapiti Island since seafloor scarps in semiconsolidated, well-bedded Plio-Pleistocene rocks become heavily modified by erosional processes in the narrows [*Lewis et al.*, 1994; NIWA, unpublished data, 2005].

[44] In zone III and inshore of Kapiti Island in zone I, there is some uncertainty whether pronounced bathymetric slopes in these areas are the result solely of active deformation, or if they have been formed and modified by prevailing long-shore currents and/or waves. The close spatial relationships between these breaks in slope and the location of large offset basement structures, however, does not appear to be coincidental, as these relationships are confirmed by MCS data (Figure 2), and supports the contention that the location of these steep slopes are controlled directly by the underlying faults. These observations highlight some of the inherent difficulties with deriving earthquake source parameters, such as slip rates, from seafloor scarps. In particular, definition of the age of the seafloor is difficult, especially in areas of high erosion and/or nearshore sediment transport where fault scarp heights, and hence displacements, may be diminished or accentuated

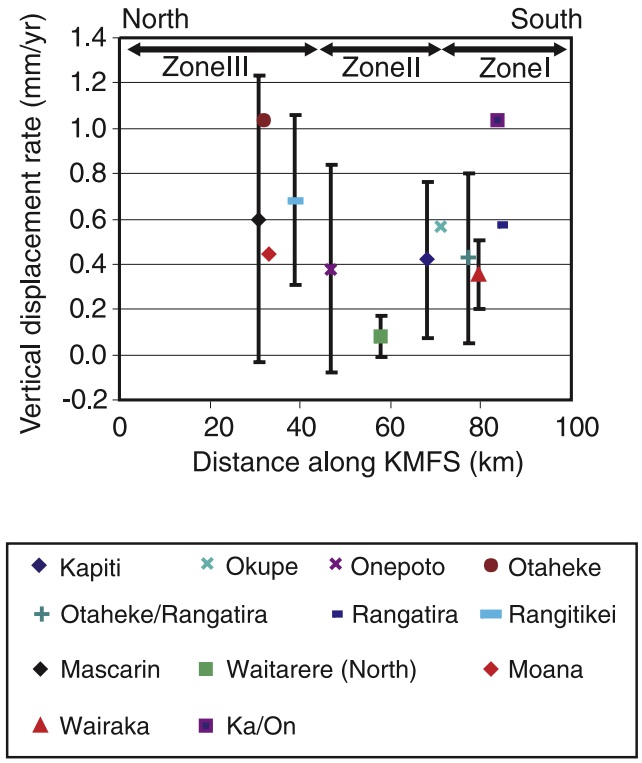

Figure 12. Vertical displacement rate (in millimeters per year, mm a^{-1}) and projected distance (in kilometers) along all faults of the KMFS over the last 11,000 a. The N23°E projection axis origin is shown on Figure 2.

by oceanographic and sedimentary processes. Therefore, in certain cases, morphologic information from seafloor scarps may provide minimum estimates of earthquake source parameters, such as in highly erosive environments, or maximum estimates where underlying structures are emphasized by sedimentary processes, such as current channeling.

[45] Across the KMFS, recent fault activity, as defined by the lateral extent of seafloor scarps (Figure 2), matches very closely the spatial patterns of long-term displacement on the faults, as represented by vertical offset on a late Quaternary horizon (H1, estimated to be 120 ka old or possibly 260 ka old [*Proust et al.*, 2005]) (Figure 13). This observation supports the assertion made by *Lamarche et al.* [2005] that fault length in the KMFS is likely to have been initiated early in the evolution of the fault zone and that fault growth was achieved largely by increases in displacement with near-constant fault lengths. The early acquisition of fault lengths in the KMFS is consistent with reactivation of preexisting extensional structures under a constant regional strain regime [*Lamarche et al.*, 2005]. In the case of the KMFS, the close spatial relationships between zones of maximum offset throughout the late Quaternary and especially the post-20 ka period (Figure 13) indicates that the reactivated reverse faults in the KMFS have behaved in a similar way to normal faults in other systems where fault growth has been facilitated mainly by increasing displacement with near-constant fault lengths. This conclusion favors fault growth models advocated by *Walsh et al.* [2002] and others [e.g., *Morewood and Roberts*, 2002; *Nicol et al.*, 2005], which had previously been applied essentially to normal fault systems, until *Lamarche et al.* [2005] demonstrated the existence of a similar pattern for reactivated reverse structures in the offshore KMFS. The present study demonstrates that this long-term behavior over the geological history of the fault also persists into recent times with similar spatial patterns observed for deformation of the post-last glacial erosion surface (10.8 a old) and the 120 or 260 a old H1 horizon (Figure 13).

5.2. Comparison of Short- and Long-Term Slip Rates

[46] The range of late Quaternary slip rates obtained for each fault in the KMFS are reasonably consistent with long-term estimates as documented over the last 120 ka (Table 3). The geological slip rates were estimated to range from 0.2 mm a^{-1} on the Wairaka Fault to 1.8 mm a^{-1} on the Mascarin Fault by *Lamarche et al.* [2005]. Typically, the minimum and maximum slip rate estimates from the neotectonic data either bracket the 120 ka values, or the long-term rates lie at the lower end of the range of values from the present study, except for the Rangitikei Fault, where the 120 ka slip rate is about 50% higher than the maximum neotectonic estimate (Table 3).

[47] The highest maximum long-term slip rates in the offshore KMFS were found on the Mascarin Fault with vertical displacement rates over the last 1.35 Ma ranging from 0.5 to −0.7 mm a^{-1} from 1350 to 120 ka, possibly increasing to 1.3 mm a^{-1} from 120 ka to present [*Lamarche et al.*, 2005]. Interpretation of late Quaternary deformation data suggests similar slip rates on the Mascarin Fault, ranging from 0.1 to 3.3 mm a^{-1} over the last ~11 ka, decreasing southward along the fault. The Onepoto and Rangitikei faults exhibit average long-term slip rates of 0.25–0.5 mm a^{-1}, with maximum rates of 1.3 and 1.5 mm a^{-1}, respectively, occurring in the last 120 ka (Table 3). The average long-term rates are comparable to the short-term rates for Onepoto (~0.1 mm a^{-1} on the southern section and 0.6 ± 0.5 mm a^{-1} on the northern section), but higher than that estimated for the Rangitikei Fault from neotectonic data (0.7 ± 0.4 mm a^{-1}, Table 3). The remaining faults within the offshore KMFS have long-term slip rates over the last 1.35 Ma of generally less than 0.2 mm a^{-1}, which seems to be overestimated by the average short-term rates of 0.4–1.1 mm a^{-1} (Table 3). The only exception is the Waitarere Fault where the geological and neotectonic slip rates are similar at ~0.1 mm a^{-1}.

[48] The observations that average and maximum short-term slip rates are higher than geological rates, possibly reflect an increase in slip rates over the last 120 ka, compared to the previous 2.5 Ma, as proposed by *Lamarche et al.* [2005]. In this regard, maximum short-term slip rates on the KMFS faults are often >1 mm a^{-1}, such that the short-term data perhaps confirm a substantial increase in the seismic hazard potential of the KMFS over the last 20 ka. There is the possibility, however, that the age of the youngest unconformity imaged on MCS profiles in the WB may be 260 ka [*Lamarche et al.*, 2005; *Proust et al.*, 2005], which would effectively halve the long-term, post-120 ka slip rates given in Table 3. This would mean that the average short-term slip rates for the last 20 ka are possibly even closer to the long-term geological estimates for some faults (e.g., Kapiti, Rangitikei), but greater than the geolog-

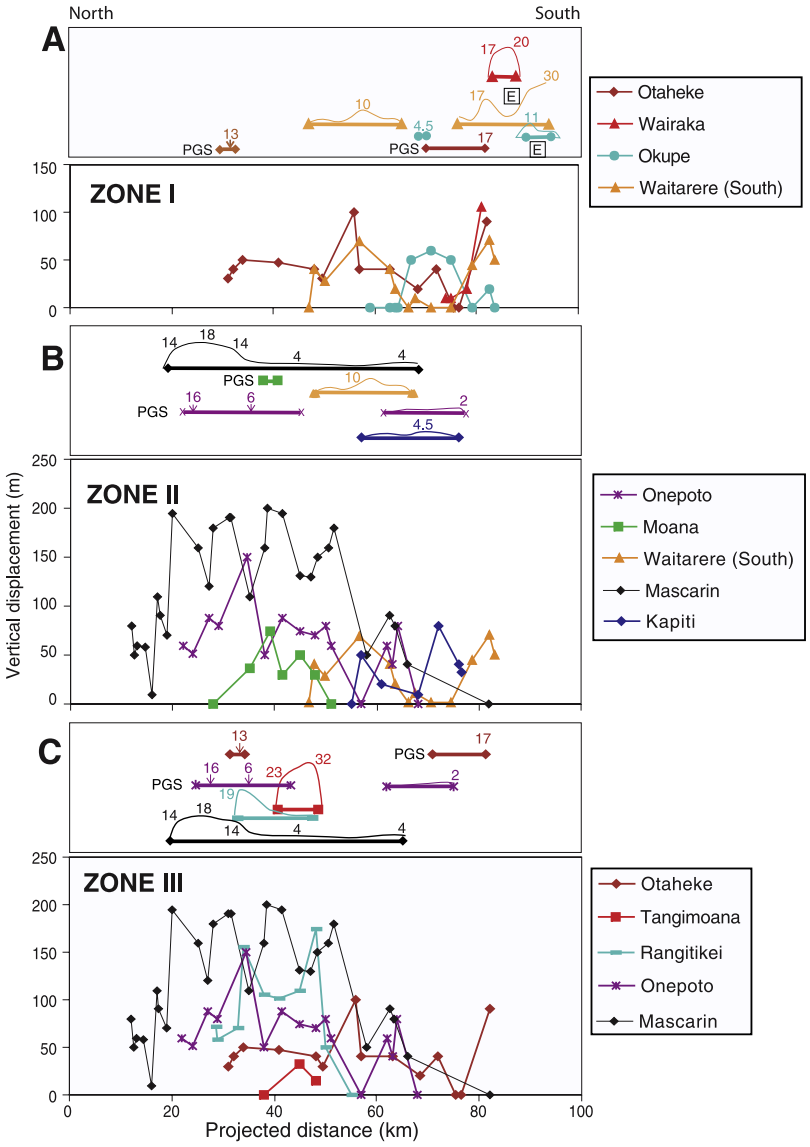

Figure 13. Vertical displacement (in meters) and projected distance (in kilometers) along all faults of the KMFS measured on horizon H1 (120 or 260 ± ~20 ka [*Lamarche et al.*, 2005; *Proust et al.*, 2005]) shown in Figures 13a (bottom), 13b (bottom), and 13c (bottom), each of which represent the neotectonic deformation zones of the KMFS for zones I, II and II, respectively (see text for details). The lateral extents of seafloor scarps and near-surface deformation (where scarps are not present) are depicted in Figures 13a (top), 13b (top), and 13c (top) for zones I, II, and III, respectively. The vertical profiles are depicted for seafloor offsets only and are scaled relative to each other. Faults are grouped in each neotectonic zone based on common fault attributes and close spatial relationships of mapped faults (see text for details). The N23°E axis origin used for calculating the projected distance is shown on Figure 2. PGS, post-last glacial erosion surface; E, eroded scarp.

ical rates estimated for others (e.g., Mascarin, Otaheke (N), Okupe, Waitarere (N)).

[49] The spatial mapping of neotectonic features in the KMFS closely matches zones of maximum offset measured on older time horizons [*Lamarche et al.*, 2005] (Figure 13). This observation indicates that the modern-day deformation is reflecting long-term trends in fault activity on the structures in the KMFS. Active faults in zone III to the north are linked to large structures mapped previously onshore, such as the Turakina, Rangitikei and possibly Rauoterangi faults [*Hunt*, 1980; *Anderton*, 1981; *Lamarche et al.*, 2005] (Figure 2). Onshore, these active faults and associated splays bound several growing, asymmetric anticlinal structures in Manawatu west of the main uplifted Axial Ranges [*Te Punga*, 1957; *Anderton*, 1981; *Melhuish et al.*, 1996; *Jackson et al.*, 1998]. The minimum and average late Quaternary and post-20 ka rates determined in the offshore KMFS are comparable with previous estimates of slip rates on the anticlinal structures (0.1–0.3 mm a^{-1} [*Melhuish et al.*, 1996]), but are closer to the lowermost estimates of the long- and short-term average slip rates in the KMFS, ranging from 0.2 to 1.8 mm a^{-1} and 0.1 to 1.0 mm a^{-1},

respectively (Table 3). Across the KMFS, the highest slip rates and seafloor offsets are found in the north in zone III before the faults pass onshore into Manawatu and in zone I to the south around Kapiti Island. In the central reaches of the KMFS in zone II, slip rates and vertical offsets are more subdued, although the occurrence of seafloor scarps and displacements on near-surface reflectors is more definitive than to the north and south where there is some ambiguity in interpretation (Figure 2).

5.3. Earthquake Source Parameterization

5.3.1. Seafloor Offsets and Fault Seafloor Rupture Lengths

[50] Near-surface deformation data indicate that fault seafloor rupture lengths within the KMFS are generally 10–20 km with a maximum of about 50 km estimated for the Mascarin Fault (Table 3). Onshore expression of active faults and folds in lower North Island are also of this order, ranging from <5 to ~20 km lengths [e.g., *Melhuish et al.*, 1996; *van Dissen and Berryman*, 1996; *Heron et al.*, 1998; *Jackson et al.*, 1998] and up to 55 km as estimated for the Ohariu Fault [*Litchfield et al.*, 2004] to a maximum of 90 km, including the North Ohariu section [*Stirling et al.*, 2002a]. Fault lengths based on seafloor rupture characteristics in the KMFS are on average ~50% less than those estimated from the subsurface lateral extent of the fault determined from deep geophysical studies (Table 3). This observation is consistent with other interpretations of the rupture characteristics of historical earthquakes, where it is recognized that seafloor rupture length is generally shorter than the subsurface rupture length for a given earthquake [e.g., *Stirling et al.*, 2002a]. Perhaps these observations indicate that (1) $L_{subsurface}$ is representative of fault rupture over much longer time periods than those represented by seafloor ruptures, (2) $L_{subsurface}$ approximates the location of surface-rupturing earthquake events that occur on what are essentially continuous or linked faults at depth [e.g., *Walsh et al.*, 2003], or (3) the surface expression of a fault only accounts for a small part of the maximum extension due to the ellipsoidal shape of faults [*Kim and Sanderson*, 2005], although given that the subsurface depths from which such lengths are calculated are relatively shallow, curvature of elliptical tip lines is unlikely to fully account for this factor.

[51] Seafloor fault scarps in the KMFS range from 2.3 to 30 m in height (Table 3). As discussed previously, based on observations of onshore [*van Dissen and Berryman*, 1996; *Heron et al.*, 1998] and offshore faults in the region [*Nodder*, 1993, 1994; *Nicol et al.*, 2005], it is likely that the highest scarps in the KMFS on the seafloor (i.e., those >5 m high) represent multiple paleoearthquake surface-rupturing events. Since the subsurface data resolution is not sufficient to determine individual earthquake offsets, this interpretation was tested using the empirical relationships between fault length and displacement of *Wells and Coppersmith* [1994]. This analysis indicates that the expected surface offsets in the KMFS, based on seafloor rupture length, are considerably lower (by ~2–100×) than those actually measured across all the KMFS faults (data not shown, available upon request), which supports the assertion that the larger KMFS scarps probably represent multiple earthquake surface-rupturing events.

5.3.2. Estimates of M_w Using Empirical Relations

[52] Earthquake moment magnitudes (M_w) of 5.7 to 7.5 are calculated for the KMFS using an empirical approach with equations from *Villamor et al.* [2001] and *Berryman et al.* [2002] (Table 4). This analysis assumes that the observed seafloor ruptures on faults in the KMFS behave characteristically, in that the faults rupture in a similar manner along their entire length or along individual fault segments during a single earthquake.

[53] Since $M_w \leq 6.5$ are unrealistic based on fault aspect ratios (see footnote i in Table 4), these data are excluded from further analysis. Reducing the fault width of earthquake sources with M_w between 5.7 and 6.5 so that the aspect ratio is equal or greater than 1 may not be appropriate because this would imply a seismogenic zone of ~6 km, which is unsubstantiated from seismological and geological studies in the region [*Smith*, 1979; *Garrick and Gibowicz*, 1983; *Townsend*, 1998]. In any case, reducing fault width to an aspect ratio = 1 for faults with short rupture lengths would result in only a small reduction in M_w but a commensurate decrease in recurrence interval.

[54] Excluding those data sources where $M_w \leq 6.5$ suggests an overall mean M_w for all potential earthquake fault sources in the KMFS of 6.9 ± 0.3 (±1 standard deviation, n = 52 from minimum, preferred and maximum moment magnitudes given in Table 4). Including those faults where $M_w \leq 6.5$ and assuming an aspect ratio of 1, only changes this average by 0.3 magnitude points to 6.6 ± 0.6. Average M_w calculated for faults within the deformation structural zones proposed above are similar (e.g., zone I: 6.9 ± 0.2, n = 12, zone II: 7.0 ± 0.3, n = 22, zone III: 6.9 ± 0.3, n = 24). For comparative purposes, a number of previous empirical relationships were used to estimate M_w (Figure 14), and average M_w values were also calculated for each of the faults, ranging from 6.0 ± 0.2 (1 standard deviation, n = 12) on the Otaheke-Rangatira Fault to 7.3 ± 0.1 (n = 12) on the Mascarin Fault (data not shown, available upon request). In general, estimates of M_w made using fault area, fault length, slip rate, seismic moment and single-event displacements were similar (Figure 14).

[55] *Hemphill-Haley and Weldon* [1999] described a statistical approach that used point estimates of surface fault offsets to determine prehistoric earthquake rupture events and to propose upper and lower bounds of potential earthquake magnitude, based on the *Wells and Coppersmith* [1994] relations between magnitude and average displacement. This statistical approach probably warrants wider application in the offshore environment since in many instances only the dimensions of vertical seafloor offsets can be ascertained along a seabed fault scarp. In applying this technique to the KMFS, however, only the Kapiti and Rangitikei faults can be used because only they satisfactorily meet the sampling criteria suggested by *Hemphill-Haley and Weldon* [1999]. In particular, for these two faults there was approximately 100% sample coverage along each fault rupture length with more than three to five measurements of surface displacement along the fault; actually n = 6 and 5, respectively, representing 86% and 95% coverage for the two faults. On the basis of these measurements earthquake magnitudes of 6.8–7.7 and 6.8–7.4 are calculated for the Kapiti and Rangitikei faults, respectively.

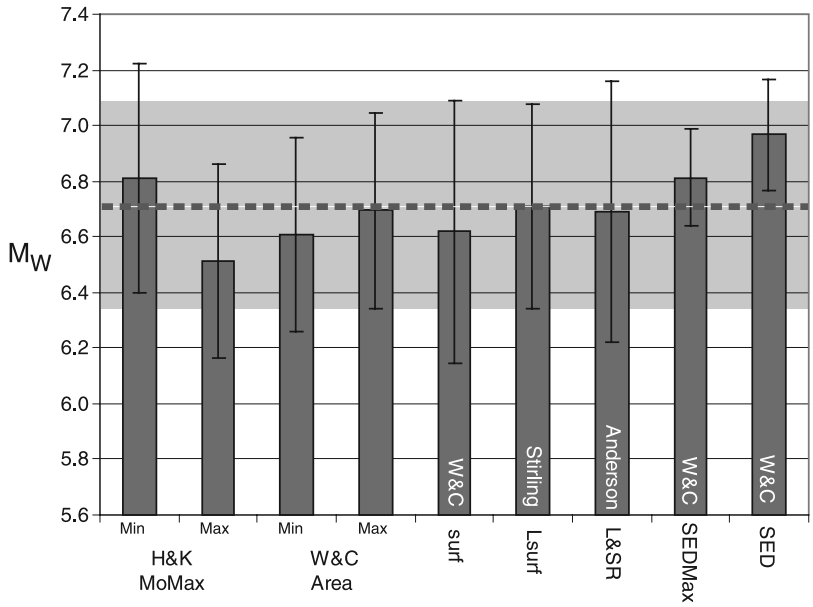

Figure 14. Moment magnitude (M_w) estimates determined from a range of empirical equations and across all faults in the KMFS. Mean $M_w \pm 1$ standard deviation for each method are depicted. The overall mean and standard deviation range of M_w calculated using all methods across all faults in the KMFS where estimated $M_w \geq 6.5$ are also shown (dashed line and shaded area). Only those faults with $M_w \geq 6.5$ were used here because mapped fault lengths L < 10 km result in unrealistic fault aspect ratios (L/Depth of seismogenic zone is 15 km) of < 1, and it is assumed that surface fault ruptures are generally associated with earthquakes with $M_w > 6.5$ [e.g., *Stirling et al.*, 2002b]. The following empirical equations were used in the mean calculations (details available from the authors upon request): (1) this study–area: $M_w = 3.39 + 1/33\log_{10}(A)$ for normal faults [*Villamor et al.*, 2001] and $M_w = 4.18 + 2/3\log_{10}(W) + 4/3\log_{10}(L)$ for reverse and reverse-oblique faults [*Berryman et al.*, 2002], where A = fault area, W = fault width based on fault length (L), assuming a fault dip of 70° (as detailed in Tables 3 and 4). (2) H&K–MoMax: $M = {}^2/_3\log_{10}(M_oMax) - 10.7$ from *Hanks and Kanamori* [1979]; M_oMax is maximum seismic moment from Table 4. (3) W&C–area: $M = 4.33 + 0.90[\log_{10}(A)]$ for reverse faults ($r^2 = 0.94$) from *Wells and Coppersmith* [1994]; Min is minimum (seismogenic depth = 13 km) and Max is maximum (seismogenic depth = 17 km) (see text for details). (4) W&C–L_{surf}: $M = 5.00 + 1.22[\log_{10}(L)]$ for reverse faults ($r^2 = 0.88$) from *Wells and Coppersmith* [1994], L_{surf} is seafloor rupture length (L) in Tables 3. (5) Stirling–L_{surf}: $M_w = 5.45 + 0.95[\log_{10}(L)$ from *Stirling et al.* [2002a]. (6) Anderson–L&SR: $M_w = 5.12 + 1.16[\log_{10}(L)] - 0.20[\log_{10}(SR)]$ for all faults, standard deviation of 0.26 magnitude units, from *Anderson et al.* [1996], SR is slip rate as in Tables 3. (7) W&C–SEDMax: $M_w = 6.69 + 0.74[\log_{10}(SEDMax)]$ for all faults ($r^2 = 0.78$) from *Wells and Coppersmith* [1994] since the W&C regression for reverse faults was not significant (at 95% CI) ($r^2 = 0.36$); SEDMax is maximum single-event displacement as in Table 4. (8) W&C–SED: $M_w = 6.93 + 0.82[\log_{10}(SED)]$ for all faults ($r^2 = 0.75$) from *Wells and Coppersmith* [1994] since the W&C regression for reverse faults was not significant (at 95% CI) ($r^2 = 0.10$).

[56] *Stirling et al.* [1998] and *Dowrick and Rhoades* [2004] suggest that magnitudes predicted using multiregion relations, as devised by *Wells and Coppersmith* [1994], underestimate earthquake magnitudes by ~0.4 units compared with New Zealand-based data. Thus the values proposed in Figure 14 using Wells and Coppersmith equations for the KMFS are probably conservative values. While the Wells and Coppersmith empirical relations are not regarded as widely applicable to New Zealand faults, they are included here as a means of comparing different historical methods for estimating M_w. Given the surface expression of fault rupture in the KMFS over relatively short segments (i.e., approximately 10–20 km lengths, with inferred single-displacement event scarp heights generally 1–5 m, Table 3), and the observations of only moderate-sized crustal earthquakes in the Wanganui-Manawatu area [*Garrick and Gibowicz*, 1983], it seems that the magnitude estimates based on the empirical equations used in this study are about of the right order. Consistent with our interpretations, are the observations made by *Melhuish et al.* [1996] suggesting magnitudes of M 6.5–7+ for late Quaternary reverse deformation of the onshore Mount Stewart-Halcombe Anticline. This structure is likely to be cored by reverse faults that link laterally to the offshore faults of the KMFS [e.g., *Lamarche et al.*, 2005], and therefore earthquake mechanisms and rupture characteristics could be regarded as similar. Furthermore, *Stirling et al.* [1998] suggested that other active anticlines in southeastern North Island could be associated with earthquakes over a wide range of magnitudes (M_w 6.2–7.1).

5.3.3. Recurrence Intervals

[57] KMFS faults exhibit a wide range of recurrence intervals, ranging from minimum values of 100–400 a to maximums >100,000 a (Table 4). An average estimate for the minimum recurrence interval is 1400 a and for the maximum, 33,000 a. The lowest average recurrence intervals of <5000 a were estimated for the Kapiti, Okupe (northern section), central and northern Onepoto, Otaheke, Otaheke-Rangatira, Rangitikei, Wairaka and Mascarin (northern section) faults, rising to >10,000 a on most of the other faults in the KMFS. This range of recurrence intervals for the KMFS as a whole reflects the uncertainties surrounding estimates of surface displacement and slip rate. In particular, many surface offsets on the faults are most likely the result of multiple earthquake events, and well-constrained slip rate data were not consistently obtainable for all the structures in the KMFS (see methods).

[58] These late Quaternary approximations of earthquake recurrence intervals are, however, similar to those determined for onshore neotectonic structures in Manawatu (e.g., several thousand years to >10,000 a [*Melhuish et al.*, 1996; *Stirling et al.*, 1998]), while the lowest recurrence intervals are similar to those determined for active strike-slip faults in the adjacent southern North Island, such as the Ohariu and Shepherd Gully faults (1500–7000 a [*van Dissen and Berryman*, 1996; *Stirling et al.*, 1998]).

5.3.4. Seismic Hazard Implications of Recent Faulting in the KMFS

[59] With some maximum recurrence intervals estimated to be >100,000 a for several faults in the offshore KMFS, the seismic hazard in the Manawatu-Wanganui region is regarded justifiably as "low" [*Smith and Berryman*, 1986; *Stirling et al.*, 1998, 2002b]. For numerous KMFS faults, however, such as the Kapiti, the northern section of Okupe, Otaheke-Rangatira, Rangitikei and the Mascarin faults, average recurrence intervals could be of the same order as those estimated for the strike-slip faults located further to the south, such as the Ohariu, Shepherds Gully/Pukerua and Wairau faults (i.e., 1500–7000 a [e.g., *van Dissen and Berryman*, 1996; *Heron et al.*, 1998; *Stirling et al.*, 1998; *Litchfield et al.*, 2004]). In addition, the present study has not taken into account the possibility that there might be some oblique slip activity on the KMFS faults [*Lamarche et al.*, 2005], which would result in increased slip rates, which would then reduce the estimated recurrence intervals for the offshore faults.

[60] Since earthquakes of magnitude five and above can cause significant damage to buildings, and even injuries and deaths, there is still potential for the faults within the KMFS to contribute to earthquake hazard in the Kapiti-Manawatu region. For example, moderate magnitude earthquakes occur in the region as indicated by historical data (e.g., M 6.5 earthquake off Wanganui in 1897 (G. Downes and D. J. Dowrick, personal communication, 2006)) and by a M 6.5 earthquake off the Manawatu coast in 1991 that resulted in over 2000 damage claims to the New Zealand Earthquake Commission (Wanganui District Council Web site http://www.wanganui.govt.nz/civilDef/earthquake.html#history). Possible tsunami deposits have also been recognized onland on Kapiti Island, possibly resulting from surface rupturing on nearby offshore faults [*Goff et al.*, 2000], and local or regional tsunami have been interpreted as being responsible for disrupting prehistoric human occupation along the Kapiti coastline since 13th century A.D. [*Goff and McFadgen*, 2003].

[61] Along the Kapiti-Manawatu coast, peak ground accelerations calculated in preliminary updates of the National Seismic Hazard model for a 475 a return period (i.e., a 10% probability of exceedance in 50 a) show a near doubling from 0.4–0.5 g, as documented previously by *Stirling et al.* [2002b], to 0.5–0.7 g when the model was parameterized using fault and paleoseismic data parameters determined by the present study (Figure 15). In the work by *Stirling et al.* [2002b] and subsequent unpublished model runs (Figure 15a), the only offshore structure in the Kapiti-Manawatu region has been the depiction and parameterization of the Wairau Fault as a single, long, linear feature extending from Cook Strait to the Rangitikei River mouth (~130 km in length). With new data from this study, the impact on the hazard assessment model has been an increase in the areal extent of potential seismic hazard along the Kapiti-Manawatu coast and a concentration of ground shaking within the offshore KMFS, associated mainly with the Mascarin Fault. Thus, while, in a general sense, potential earthquake magnitudes in the KMFS are only moderate (overall mean 6.9 ± 0.3, Table 4 and Figure 14) with occasional low- to moderate-return periods (<5000 to 10,000 a), it appears that further appraisal of the seismic hazard associated with offshore and onshore structures in the Kapiti-Manawatu region is warranted. This is pertinent and timely because previous workers, who have developed national seismic hazard models for New Zealand, have regarded the hazard in this region as low [*Smith and Berryman*, 1986; *Stirling et al.*, 1998, 2002b].

6. Conclusions

[62] 1. Seafloor scarps and deformation of post-last glacial sediments indicate recent activity on faults in the low-strain, compressional Kapiti-Manawatu Fault System, offshore southern North Island, New Zealand.

[63] 2. Scarps vary in height from 1 to 30 m and up to 50 km in length and are closely aligned with loci of maximum uplift on deeper structures mapped with multichannel seismic reflection data previously by *Lamarche et al.* [2005]. Slip rates on the KMFS faults are comparable to long-term rates and published estimates from onshore studies.

[64] 3. Three main zones of offshore neotectonic deformation are recognized (essentially from north to south): (1) zone I around Kapiti Island is characterized by large, often eroded seafloor scarps (~10–30 m high) with low slip rates (<0.4 mm a^{-1}) (e.g., Waitarere (S), Okupe (S), Otaheke-Rangatira and Wairaka faults); (2) zone II has moderately high scarps (~1–5 m high) and low to very low slip rates (<0.2 mm a^{-1}), except on the Kapiti Fault, with maximum slip rates of 2 mm a^{-1} (e.g., Kapiti, Waitarere (N), Onepoto (S), Okupe (N) and Mascarin (S) faults); and (3) zone III represents the most active structures in the KMFS with prominent bathymetric changes in seafloor slope (>10 m high scarps) and moderate to high slip rates (>0.1–3.0 mm a^{-1}) (e.g., Mascarin (N), Onepoto (N), Rangitikei, Otaheke and Tangimoana faults).

[65] 4. Earthquake moment magnitudes, seismic moments and single-event displacements for individual structures in

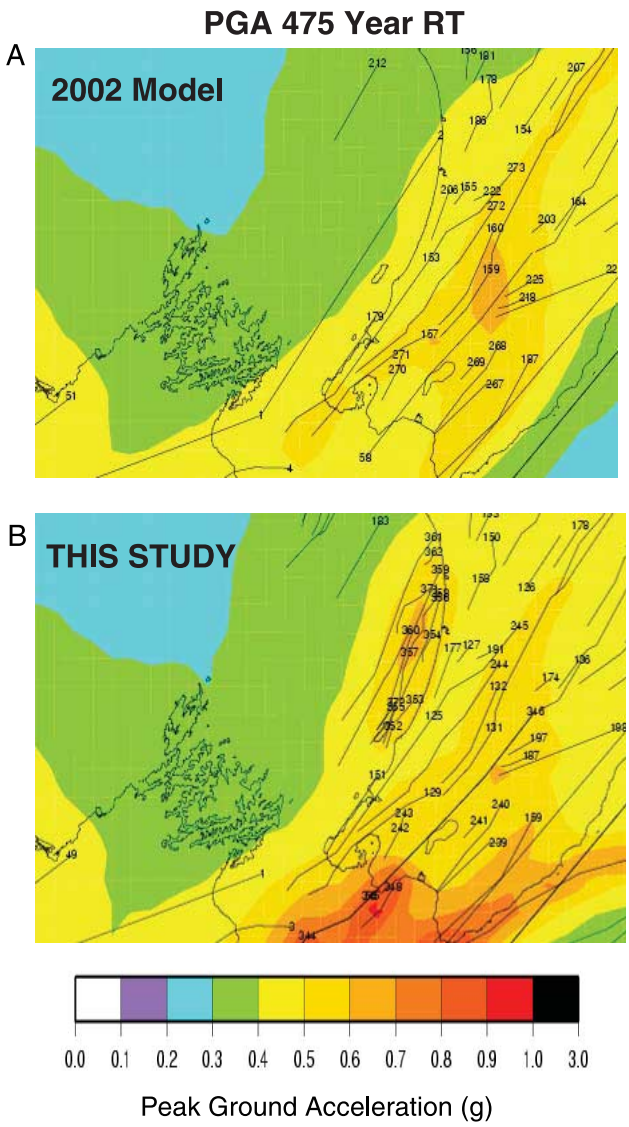

Figure 15. Preliminary implications of KMFS earthquake recurrence estimates as input parameters to the National Seismic Hazard Assessment model [*Stirling et al.*, 2002b]. (a) Distributions of faults (thin lines) and peak ground acceleration (PGA, contours) with a 475 a return time period for southern North Island from an unpublished 2002 study. These PGA values are equivalent to the maximum acceleration expected with a 10% probability of being exceeded in 50 a and assume site class B intermediate soil conditions, which have natural periods of 0.6 s in the response spectrum attenuation model. (b) Preliminary run of the same model with new fault parameters from the offshore KMFS (this study).

the KMFS are estimated from empirical equations. M_w ranges from 5.8 to 7.5 (mean 6.7 ± 0.4), with highly variable M_o estimates and SEDs in the range of 0.9–1.7 m. Excluding unrealistic values ≤6.5, results in an overall mean M_w of 6.9 ± 0.3. Recurrence intervals are also variable with RIs as low as 100 a and as high as >100,000 a. On average, however, RIs for earthquakes on several of the more prominent structures in the offshore, largely reverse KMFS are comparable to published estimates for onshore reverse and strike-slip structures.

[66] 5. Since the KMFS faults could generate moderate to high moment magnitude earthquakes (M_w 6–7), but at reasonably long recurrence intervals (>5000 a), the seismic hazard of the region is likely to remain regarded as "low." A preliminary reapplication, however, of the National Seismic Hazard Assessment model [*Stirling et al.*, 2002b], indicates that peak ground accelerations with a 475 a return period on the KMFS faults would effectively double along the Kapiti-Manawatu coast using the neotectonic fault parameters in the present study.

[67] Offshore neotectonic deformation is often integrated poorly into regional seismic hazard analyses, with the consequence that the hazard associated with active faulting may be underestimated. The approach presented here provides a method for evaluating the potential hazards associated with offshore active structures, using the reactivated reverse and normal faults of the Kapiti-Manawatu Fault System, southern North Island, New Zealand, as examples.

[68] The approach undertaken in the present paper has demonstrated the potential to evaluate and quantify the seismic hazard associated with offshore, steep, reactivated reverse faults. Previously, similar approaches have been applied to normal [*Nodder*, 1993, 1994; *Bull et al.*, 2006] and thrust faults [*Barnes et al.*, 2002] on the New Zealand continental shelf. The approach therefore shows considerable promise for more widespread application in other regions where faulting hazards are likely to be underestimated by neglecting to account for active deformation in adjacent offshore environments.

[69] **Acknowledgments.** We are grateful to Miles Dunkin (NIWA) for digitizing and preparing the structural maps and to Brett Grant and Erika McKay (NIWA) for redrafting the figures. David Dowrick (Institute of Geological and Nuclear Sciences (GNS Science) Ltd) kindly provided a preprint of a submitted manuscript that aided our paleoseismic interpretations, as did personal communications with Gaye Downes and David D. (also GNS Science). Thanks to Jeanette Gillespie (deceased), Avon McIntyre (both University of Waikato), and Alan Beu (GNS Science) for mollusk and Daphne Lee (University of Otago) for brachiopod identifications prior to radiocarbon dating. Sample dating was undertaken at the Radiocarbon Dating Laboratory, University of Waikato, and at the Accelerator Mass Spectrometer facility, GNS Science Rafter Radiocarbon Laboratory, New Zealand. Helen Neil (NIWA) helped with the ^{14}C age calibrations. Biostratigraphic data analysis and interpretations were conducted by Tony Edwards at Stratigraphic Solutions (New Zealand) Ltd. Comments from one of the journal reviewers helped tighten aspects of the discussion, thereby improving the paper. International travel, as part of this New Zealand–French collaboration, was facilitated by a grant from the French Ministry of Foreign Affairs, allocated by the Services Scientifiques of the French Embassy in Wellington, New Zealand, and by NIWA as part of a partially NSOF-funded sabbatical for S.D.N. to Géosciences Rennes in 2004–2005. This 3-month sabbatical and a yearlong one at NIWA by J.-N.P. in 2002–2003 were also funded by the Centre National de la Recherche Scientifique (CNRS, France). The work was completed as part of the FRST-funded program Consequences of Earth-Ocean Change (C01X0203).

References

Aharoni, E. (1991), Seismic reflection study across the Horowhenua coastal plain, North Island, New Zealand, M. Sc. thesis, 169 pp., Victoria Univ. of Wellington, Wellington, New Zealand.

Aki, K., and P. G. Richards (1980), Quantitative Seismology: Theory and Methods, W. H. Freeman, San Francisco, California.

Alloway, B. V., et al. (2007), Towards a climate event stratigraphy for New Zealand over the last 30,000 years (NZ-INTIMATE project), *J. Quat. Sci.*, *22*, 9–35.

Anderson, J. G., S. G. Wesnousky, and M. W. Stirling (1996), Earthquake size as a function of fault slip rate, *Bull. Seismol. Soc. Am.*, *86*, 683–690.

Anderton, P. W. (1981), Structure and evolution of the South Wanganui Basin, New Zealand, *N. Z. J. Geol. Geophys.*, *24*, 39–63.

Ansell, J. H., and S. C. Bannister (1996), Shallow morphology of the subducted Pacific plate along the Hikurangi margin, New Zealand, *Phys. Earth Planet. Inter.*, *93*, 3–20.

Barnes, P. M., A. Nicol, and T. Harrison (2002), Late Cenozoic evolution and earthquake potential of an active listric thrust complex above the Hikurangi subduction zone, New Zealand, *Geol. Soc. Am. Bull.*, *114*, 1379–1405, doi:10.1130/0016-7606 [2002]114<1379:LCEAEP>2.0.CO;2.

Beanland, S. (1995), The North Island Dextral Fault Belt, Hikurangi subduction margin, New Zealand, Ph.D. thesis, 341 pp., Victoria Univ. of Wellington, Wellington, New Zealand.

Berryman, K., T. Webb, N. Hill, M. Stirling, D. Rhoades, J. Beavan, and D. Darby (2002), Seismic loads on dams: Waitaki system—Earthquake source characterization, *GNS Client Rep. 2001/129*, GNS Sci., Lower Hutt, New Zealand.

Bonilla, M. G., R. K. Mark, and J. J. Lienkaemper (1984), Statistical relations among earthquake magnitude, surface rupture length, and surface fault displacement, *Bull. Seismol. Soc. Am.*, *74*, 2379–2411.

Brune, J. N. (1968), Seismic moment, seismicity, and rate of slip along major fault zones, *J. Geophys. Res.*, *73*, 777–784.

Bull, J. M., P. M. Barnes, G. Lamarche, D. J. Sanderson, P. A. Cowie, J. K. Dix, and S. Taylor (2006), High-resolution record of displacement accumulation on an active normal fault: Implications for models of slip accumulation during repeated earthquakes, *J. Struct. Geol.*, *28*, 1146–1166, doi:10.1016/j.jsg.2006.03.006.

Busby, C. J., and R. V. Ingersoll (Eds.) (1995), *Tectonics of Sedimentary Basins*, 579 pp., Blackwell, Oxford, U.K.

Carter, L. (1992), Acoustical characterisation of seafloor sediments and its relationship to active sedimentary processes in Cook Strait, New Zealand, *N. Z. J. Geol. Geophys.*, *35*, 289–300.

Carter, L., K. B. Lewis, and F. J. Davey (1988), Faults in Cook Strait and their bearing on the structure of central New Zealand, *N. Z. J. Geol. Geophys.*, *31*, 431–446.

Carter, R. M., and T. R. Naish (1998), A review of Wanganui Basin, New Zealand: Global reference section for shallow marine, Plio-Pleistocene (2.5–0 Ma) cyclostratigraphy, *Sediment. Geol.*, *122*, 37–52.

Carter, R. M., L. Carter, and D. P. Johnson (1986), Submergent shorelines in the SW Pacific: Evidence for an episodic post-glacial transgression, *Sedimentology*, *33*, 629–649.

Cornell, C. A. (1968), Engineering seismic risk analysis, *Bull. Seismol. Soc. Am.*, *58*, 1583–1606.

Cowie, J. D. (1963), Dune-building phases in the Manawatu district, New Zealand, *N. Z. J. Geol. Geophys.*, *6*, 268–280.

De Mets, C., R. G. Gordon, D. F. Argus, and S. Stein (1994), Effect of recent revisions to the geomagnetic reversal time scale on estimates of current plate motions, *Geophys. Res. Lett.*, *21*, 2191–2194.

DePolo, C. M., and D. B. Slemmons (1990), Estimation of earthquake size for seismic hazards, in *Neotectonics in Earthquake Evaluation*, *Rev. Eng. Geol.*, vol. 8, edited by E. L. Krinitsky and D. B. Slemmons, pp. 1–28, Geol. Soc. of Am., Boulder, Colo.

Doser, D. I., and T. H. Webb (2003), Source parameters of large historical (1917–1961) earthquakes, North Island, New Zealand, *Geophys. J. Int.*, *152*, 795–832.

Dowrick, D. J., and D. A. Rhoades (2004), Relations between earthquake magnitude and fault rupture dimensions: How regionally variable are they?, *Bull. Seismol. Soc. Am.*, *94*, 776–788.

Dunbar, G. B., and P. J. Barrett (2005), Estimating palaeobathymetry of wave-graded continental shelves from sediment texture, *Sedimentology*, *52*, 253–269.

Eiby, G. A. (1968), An annotated list of New Zealand earthquakes 1460–1965, *N. Z. J. Geol. Geophys.*, *11*, 630–647.

Fleming, C. A. (1953), The geology of Wanganui subdivision; Waverley and Wanganui sheet districts (N137 and N138), *N. Z. Geol. Surv. Bull.*, *52*, 372 pp, GNS Science, Lower Hutt, New Zealand.

Garrick, R. A., and S. J. Gibowicz (1983), Continuous swarm-like seismicity: The Wanganui, New Zealand, earthquakes, *Geophys. J. R. Astron. Soc.*, *75*, 493–512.

Gibb, J. G. (1986), A New Zealand regional Holocene eustatic sea-level curve and its application to determination of vertical tectonic movements—A contribution to IGCP-Project 200, *Bull. R. Soc. N. Z.*, *24*, 377–395.

Gillespie, J. L., C. S. Nelson, and S. D. Nodder (1998), Post-glacial sea-level control and sequence stratigraphy of carbonate-terrigenous sediments, Wanganui shelf, New Zealand, *Sediment. Geol.*, *122*, 245–266.

Goff, J. R., and B. G. McFadgen (2003), Large earthquakes and the abandonment of prehistoric coastal settlements in 15th century New Zealand, *Geoarchaeology*, *18*, 609–623.

Goff, J. R., H. L. Rouse, S. L. Jones, B. W. Hayward, U. Cochran, W. McLea, W. W. Dickinson, and M. S. Morley (2000), Evidence of an earthquake and tsunami about 3100–3400 years ago, and other catastrophic saltwater inundations recorded in a coastal lagoon, New Zealand, *Mar. Geol.*, *170*, 231–249.

Grapes, R., and G. Downes (1997), The 1855 Wairarapa, New Zealand earthquake—Analysis of historical data, *Bull. N. Z. Natl. Soc. Earthquake Eng.*, *30*, 271–368.

Hanks, T. C., and H. Kanamori (1979), A moment magnitude scale, *J. Geophys. Res.*, *84*, 2348–2350.

Hemphill-Haley, M. A., and R. J. Weldon (1999), Estimating prehistoric earthquake magnitude from point measurements of surface rupture, *Bull. Seismol. Soc. Am.*, *89*, 1264–1279.

Heron, D., R. van Dissen, and M. Sawa (1998), Late Quaternary movement on the Ohariu Fault, Tongue Point to MacKays Crossing, North Island, New Zealand, *N. Z. J. Geol. Geophys.*, *41*, 419–439.

Herzer, R. H. (1981), Late Quaternary stratigraphy and sedimentation of the Canterbury continental shelf, New Zealand, *N. Z. Oceanogr. Inst. Mem.*, 89, 71 pp.

Holt, W. E., and T. A. Stern (1994), Subduction, platform subsidence, and foreland thrust loading: The late Tertiary development of Taranaki Basin, New Zealand, *Tectonics*, *13*, 1068–1092.

Hunt, T. M. (1980), Basement structure of the Wanganui Basin, onshore, interpreted from gravity data, *N. Z. J. Geol. Geophys.*, *23*, 1–16.

Jackson, J., R. J. van Dissen, and K. R. Berryman (1998), Tilting of active folds and faults in the Manawatu region, New Zealand: Evidence from surface drainage patterns, *N. Z. J. Geol. Geophys.*, *41*, 377–385.

Kamp, P. J. J., A. J. Vonk, K. J. Bland, R. Funnell, A. G. Griffin, S. Hayton, A. J. W. Hendy, A. P. McIntyre, C. S. Nelson, and T. Naish (2002), Megasequence architecture of Taranaki-Wanganui-King Country basins and Neogene progradation of two continental margin wedges across western New Zealand, paper presented at the 2002 New Zealand Oil Conference, Pet. Geotherm. Unit, Energy Resour. Div., Minist. of Commer., Wellington, New Zealand.

Katz, R., and B. Leask (1990), The South Wanganui Basin—A neglected hydrocarbon prospect, *Pet. Explor. N. Z. News*, July, 19–25.

Kim, Y.-S., and D. J. Sanderson (2005), The relationship between displacement and length of faults: A review, *Earth Sci. Rev.*, *68*, 317–334, doi:10.1016/j.earscirev.2004.06.003.

Lamarche, G., J.-N. Proust, and S. D. Nodder (2005), Long-term slip rates and fault interactions under low contractional strain, Wanganui Basin, New Zealand, *Tectonics*, *24*, TC4004, doi:10.1029/2004TC001699.

Lamarche, G., P. M. Barnes, and J. M. Bull (2006), Faulting and extension rate over the last 20000 years in the offshore Whakatane Graben, New Zealand continental shelf, *Tectonics*, *25*, TC4005, doi:10.1029/2005TC001886.

Lamb, S. H., and P. Vella (1987), The last million years of deformation in part of the New Zealand plate-boundary zone, *J. Struct. Geol.*, *9*, 877–891.

Lewis, K. B., L. Carter, and F. J. Davey (1994), The opening of Cook Strait: Interglacial tidal scour and aligning basins at a subduction to transform plate edge, *Mar. Geol.*, *116*, 293–312.

Litchfield, N., R. J. van Dissen, R. Langridge, D. Heron, and C. Prentice (2004), Timing of the most recent surface rupture event on the Ohariu Fault near Paraparaumu, New Zealand, *N. Z. J. Geol. Geophys.*, *47*, 123–127.

Melhuish, A., R. J. Van Dissen, and K. R. Berryman (1996), Mount Stewart-Halcombe Anticline: A look inside a growing fold in the Manawatu region, New Zealand, *N. Z. J. Geol. Geophys.*, *39*, 123–133.

Mills, C. (1990), Gravity expression of the Patea-Tongaporutu High and subsequent model for the Taranaki Bagin margin, paper presented at 1989 New Zealand Exploration Conference, Pet. and Geotherm. Unit, Energy and Resour. Div., Minist. of Commer., Wellington, New Zealand.

Moore, P. R., and D. A. Francis (1988), Geology of Kapiti Island, central New Zealand, 23 pp., N. Z. Geol. Surv., Lower Hutt.

Morewood, N. C., and G. P. Roberts (2002), Surface observations of active normal fault propagation: Implications for growth, *J. Geol. Soc. London*, *159*, 263–272.

Muckersie, C., and M. J. Sheperd (1995), Dune phases as time-transgressive phenomena, Manawatu, New Zealand, *Quat. Int.*, *26*, 61–67.

Naish, T. R., R. M. Carter, and B. J. Pillans (1999), High resolution chronology for the Plio-Pleistocene, Wanganui Basin, New Zealand, in *The High Resolution Chronostratigraphic and Sequence Stratigraphic Record of the Plio-Pleistocene, Wanganui Basin, New Zealand*, *Inst. Geol. Nucl. Sci. Folio Ser.*, vol. 2, version 1999.1, edited by R. M. Carter and T. R. Naish, wall chart, GNS Sci., Lower Hutt, New Zealand.

Nicol, A., and J. Beavan (2003), Shortening of an overriding plate and its implications for slip on a subduction thrust, central Hikurangi Margin, New Zealand, *Tectonics*, *22*(6), 1070, doi:10.1029/2003TC001521.

Nicol, A., J. Walsh, K. Berryman, and S. Nodder (2005), Growth of a normal fault by the accumulation of slip over millions of years, *J. Struct. Geol.*, *27*, 327–342.

Nodder, S. D. (1993), Neotectonics of the offshore Cape Egmont Fault Zone, Taranaki Basin, *N. Z. J. Geol. Geophys.*, *36*, 167–184.

Nodder, S. D. (1994), Characterizing potential offshore seismic sources using high-resolution geophysical and seafloor sampling programs: An example from Cape Egmont fault zone, Taranaki shelf, New Zealand, *Tectonics*, *13*, 641–658.

Norris, R. M., and T. L. Grant-Taylor (1989), Late Quaternary shellbeds, western shelf, New Zealand, *N. Z. J. Geol. Geophys.*, *32*, 343–356.

Pillans, B., M. McGlone, A. Palmer, D. Mildenhall, B. Alloway, and G. Berger (1993), The Last Glacial Maximum in central and southern North island, New Zealand: A paleoenvironmental reconstruction using the Kawakawa Tephra Formation as a chronostragraphic marker, *Palaeogeogr. Palaeoclimatol. Palaeoecol.*, *101*, 283–304.

Proctor, R., and L. Carter (1989), Tidal and sedimentary response to the late Quaternary closure and opening of Cook Strait, New Zealand: Results from numerical modelling, *Paleoceanography*, *4*, 167–180.

Proust, J.-N., G. Lamarche, S. Nodder, and J. J. Peter Kamp (2005), Plio-Pleistocene sedimentary architecture of a proto back-arc basin: South Wanganui Basin, New Zealand, *Sediment. Geol.*, *181*, 107–145.

Reyners, M. (1998), Plate coupling and the hazard of large subduction thrust earthquakes at the Hikurangi subduction zone, New Zealand, *N. Z. J. Geol. Geophys.*, *41*, 343–354.

Robinson, R. (1986), Seismicity, structure and tectonics of the Wellington region, New Zealand, *Geophys. J. R. Astron. Soc.*, *87*, 379–409.

Schwartz, D. P., and K. J. Coppersmith (1986), Seismic hazards: New trends in data analysis using geologic data, in *Active Tectonics*, chaired by R. E. Wallace, pp. 215–230, Natl. Acad. Press, Washington, D. C.

Smith, E. G. C. (1979), A micro-earthquake survey of the Rangitikei and Manawatu Basins, *N. Z. J. Geol. Geophys.*, *22*, 473–478.

Smith, W. D., and K. R. Berryman (1986), Earthquake hazard in New Zealand: Inferences from seismology and geology, *Bull. R. Soc. N. Z.*, *24*, 223–243.

Stern, T. A., and F. J. Davey (1989), Crustal structure and origin of basins formed behind the Hikurangi subduction Zone, New Zealand, in *Origin and Evolution of Sedimentary Basins and Their Energy and Mineral Resources*, *Geophys. Monogr. Ser.*, vol. 48, edited by R. A. Price, pp. 73–86, AGU, Washington, D. C.

Stern, T. A., G. M. Quinlan, and W. E. Holt (1992), Basin formation behind an active subduction zone: Three-dimensional flexural modelling of Wanganui Basin, New Zealand, *Basin Res.*, *4*, 197–214.

Stern, T. A., G. M. Quinlan, and W. E. Holt (1993), Crustal dynamics associated with the formation of Wanganui Basin, New Zealand, in *Sedimentary Basins of the World*, vol. 2, *South Pacific Sedimentary Basins*, edited by P. F. Ballance, pp. 213–223, Elsevier, New York.

Stirling, M. W., S. G. Wesnousky, and K. R. Berryman (1998), Probabilistic seismic hazard analysis of New Zealand, *N. Z. J. Geol. Geophys.*, *41*, 355–375.

Stirling, M., D. Rhoades, and K. Berryman (2002a), Comparison of earthquake scaling relations derived from data of the instrumental and pre-instrumental era, *Bull. Seismol. Soc. Am.*, *92*, 812–830.

Stirling, M. W., G. H. McVerry, and K. R. Berryman (2002b), A new seismic hazard model for New Zealand, *Bull. Seismol. Soc. Am.*, *92*, 1878–1903.

Stuivers, M., and P. J. Reimer (1993), Extended ^{14}C database and revised CALIB radiocarbon calibration program, *Radiocarbon*, *28*, 1022–1030.

Te Punga, M. T. (1957), Live anticline in western Wellington, *N. Z. J. Sci. Technol., Sect. B*, *38*, 433–446.

Thompson, T. L., W. L. Leask, and B. T. May (1994), Petroleum potential of the South Wanganui Basin, in *1994 New Zealand Petroleum Conference Proceedings: The Post Maui Challenge—Investment and Development Opportunities*, pp. 108–127, Minist. of Commer. Energy and Resour. Div., Rotorua, New Zealand.

Townsend, T. (1998), Paleoseismology of the Waverley Fault Zone and implications for earthquake hazard in South Taranaki, New Zealand, *N. Z. J. Geol. Geophys.*, *41*, 467–474.

van Dissen, R. J., and K. R. Berryman (1996), Surface-rupture earthquakes over the last ~1000 years in the Wellington region, New Zealand, and implications for ground shaking hazard, *J. Geophys. Res.*, *101*, 5999–6019.

Villamor, P., K. Berryman, T. Webb, M. Stirling, P. McGinty, G. Downes, J. Harris, and N. Litchfield (2001), Waikato seismic loads, Task 2.1, Revision of seismic source characterization, *GNS Client Rep. 2001/59*, GNS Sci., Lower Hutt, New Zealand.

Walcott, R. I. (1987), Geodetic strain and deformational history of the North island of New Zealand during the late Cenozoic, *Philos. Trans. R. Soc. London, Ser. A*, *321*, 163–181.

Walsh, J. J., A. Nicol, and C. Childs (2002), An alternative model for the growth of faults, *J. Struct. Geol.*, *24*, 1669–1675.

Walsh, J. J., W. R. Bailey, C. Childs, A. Nicol, and C. G. Bonson (2003), Formation of segmented normal faults: A 3-D perspective, *J. Struct. Geol.*, *25*, 1251–1262.

Wells, D. L., and K. J. Coppersmith (1994), New empirical relationships among magnitude, rupture length, rupture width, rupture area, and surface displacement, *Bull. Seismol. Soc. Am.*, *84*, 974–1002.

Wesnousky, S. G. (1986), Earthquakes, Quaternary faults, and seismic hazard in California, *J. Geophys. Res.*, *91*, 12,587–12,631.

Yeats, R. S. (1986), Faults related to folding with examples from New Zealand, *R. Soc. N. Z. Bull.*, *24*, 273–292.

G. Lamarche and S. D. Nodder, NIWA Ltd, Private Bag 14-901, Kilbirnie, Wellington, New Zealand. (s.nodder@niwa.co.nz)

J.-N. Proust, Géosciences Rennes, UMR CNRS 6118, Université de Rennes 1, Campus de Beaulieu, F-35042 Rennes Cedex, France.

M. Stirling, GNS Science Ltd, P.O. Box 30-368, Lower Hutt, New Zealand.